Galactic Cosmic-Ray Anisotropy and Its Modulation in the Heliomagnetosphere, Inferred from Air Shower Observation at Mt. Norikura.

K. NAGASHIMA, K. FUJIMOTO, S. SAKAKIBARA, Z. FUJII
H. UENO, I. MORISHITA (*) and K. MURAKAMI

Cosmic-Ray Research Laboratory, Faculty of Science
Nagoya University - Nagoya 464, Japan

Summary. — Extensive air showers (EAS) with median primary energy (E_m) of $(10^{13} \div 10^{15})$ eV have been observed since 1970 at Mt. Norikura (2770 m above sea level; geographic latitude 36.1 °N, longitude 137.6 °E) in order to study a cosmic-ray sidereal daily variation of galactic origin. We report here a summary of the observed results. EAS shows a significant sidereal diurnal variation with an amplitude $(0.060 \pm 0.003)\%$ and a phase (0.8 ± 0.3) h sidereal local time for $E_m \sim 1.5 \cdot 10^{13}$ eV. Sidereal semi- and tri-diurnal variations also are statistically significant. These variations are proved to be of galactic origin by a method which uses the difference of two directional (eastward and westward) air shower observations. It is found that these variations are subject, as predicted by Nagashima *et al.*, to the annual variation due to the heliomagnetospheric modulation of the galactic anisotropy, which dominates in the rigidity region $\sim 10^{12}$ V, and further that the annual variation changes its phase due to the polarity reversal of the polar magnetic field of the Sun, which occurs at the period of the maximum solar activity. This indicates that the anisotropy is produced by the charged cosmic rays, contrary to the expectation from the γ-ray origin hypothesis suggested by Alexeenko and Navara. With the increase of E_m, the anisotropy seems to be reduced as we have not been able to detect any significant sidereal variation in EAS with $E_m \sim 2 \cdot 10^{14}$ eV. This seems contradictory to the conventional conclusion that the energy spectrum of the anisotropy is flat or slightly increases with energy.

PACS 94.40 – Cosmic rays.

(*) School of Liberal Arts, Asahi University Hozumi, Gifu 501-02, Japan.

1. – Introduction.

Cosmic-ray sidereal time variation produced from the galactic anisotropy has been studied in wide energy range by many researchers in order to obtain information on the origin of cosmic rays, their propagation in the galactic space and their modulation in the heliomagnetosphere. In 1970, we began an observation of the variation in the energy region of $\sim 10^{13}$ eV by using an air shower (AS-) array at Mt. Norikura. Prior to this, there had been many observations, of course, with underground muon telescopes in the energy region less than $\sim 10^{12}$ eV [1] and with AS-arrays in the energy region greater than $\sim 10^{13}$ eV [2-4]. The observed results, however, had been regarded to have some uncertainty owing to the heliomagnetospheric modulation of cosmic rays in case of the muon observation or to the large statistical errors involved in the AS observations and also to the atmospheric influences for both cases. Our observation at Mt. Norikura was intended so as to be almost free from these faults, as will be discussed later. The observed result was first reported in 1973, showing a significant sidereal variation with an amplitude $(0.047 \pm 0.006)\%$ and a phase (1.3 ± 0.7) hour sidereal local time [5]. Two years later, a similar result was reported by Gombosi *et al.* [6] and recently, another result showing quite a good agreement with ours has been reported by Alexeenko *et al.* [7]. Meantime, we have been observing also the directional (eastward and westward) air showers since 1974. By taking their difference, we have eliminated the atmospheric effect common to these showers and proved that 1) the difference does not show any solar diurnal variation due to anisotropies in space except for that arising from the Compton-Getting (C-G) effect due to the Earth's revolution around the Sun and that 2) its sidereal variation is produced from the same galactic anisotropy as obtained by the omnidirectional air shower observation mentioned above and, as

[1] K. NAGASHIMA and S. MORI: *Proceedings of the International Cosmic Ray Symposium on High Energy Cosmic Ray Modulation, Tokyo, Japan, 1976*, p. 326 and references therein.
[2] J. DAUDIN, P. AUGER, A. CACHON and A. DAUDIN: *Nuovo Cimento*, 3, 1017 (1956), S. SAKAKIBARA: *J. Geomagn. Geoelectr.*, 17, 99 (1965) and references therein.
[3] J. LINSLEY and A. A. WATSON: *Proceedings of the XV International Cosmic Ray Conference, Plovdiv, 1977*, 12, 203 and references therein.
[4] C. E. FICHTEL and J. LINSLEY: *Astrophys. J.*, 300, 474 (1986) and references therein.
[5] S. SAKIKIBARA, H. UENO, K. FUJIMOTO, I. KONDO and K. NAGASHIMA: *Proceedings of the XIII International Cosmic Ray Conference, Denver, 1973*, 2, 1058.
[6] T. GOMBOSI, J. KOTA, A. J. SOMOGYI, A. VRANA, B. BETEV, L. KATSARSKI, S. KAVLAKOV and I. KHIROV: *Proceedings of the XIV International Cosmic Ray Conference, München, 1975*, 2, 586.
[7] V. V. ALEXEENKO, A. E. CHUDAKOV, E. N. GULIEVA and V. G. SBORSHIKOV: *Proceedings of the XVII International Cosmic Ray Conference, Paris*, 2, 146 (1981).

a result, the latter observation also is not disturbed much by the atmospheric and solar-modulation effect [8].

Our observation has been continued in order not only to raise the statistical accuracy of the result, but also to offer evidences against the dependence of the variation on 1) the solar activity and 2) the polarity reversal of the polar magnetic field of the Sun which occurred in a period of 1979-1980. The observation has been further extended to higher-energy region in order to obtain the energy spectrum of the galactic anisotropy in the energy region of $(10^{13} \div 10^{15})$ eV. In the present paper, we summarize these results, including those reported previously [9].

2. – Air shower arrays.

AS-arrays are located at Mt. Norikura, 2770 m above sea level at geographic latitude 36.1° N and longitude 137.6° E. Average atmospheric pressure (P) and temperature (T) at the site are 723.5 mb and 2.5 °C, respectively. Their daily variations are shown in fig. 1, together with that of the wind velocity (V_W). The pressure and temperature variations at Nagoya (77 m above sea level, geographic latitude 35.2° N, longitude 137.0° E) are also shown for comparison and will be used for future reference. The AS-arrays are a part of multi-directional muon telescope installed in a house being air-conditioned and designed for protecting the snow fall on the roof, as shown in fig. 2. Material above the arrays is estimated at two cascade units in weight. The room temperature (T_R) is controlled at (22 ± 1) °C throughout the year by a heavy oil heating system and its variation within a day is kept less than 0.1 °C. So that,

[8] K. NAGASHIMA, H. UENO, K. FUJIMOTO, Z. FUJII, S. SAKAKIBARA and I. KONDO: *Proceedings of the XIV International Cosmic Ray Conference, München, 1975*, **4**, 1503.
[9] K. NAGASHIMA, K. FUJIMOTO, Z. FUJII, S. SAKAKIBARA, H. UENO and I. KONDO: *Proceedings of the XIV International Cosmic Ray Conference, München, 1975*, **4**, 1368; K. NAGASHIMA, S. SAKAKIBARA, K. FUJIMOTO, Z. FUJII, H. UENO and I. KONDO: *Proceedings of the XV International Cosmic Ray Conference, Plovdiv, 1977*, **2**, 154; K. FUJIMOTO, H. UENO, Z. FUJII, S. SAKAKIBARA, I. KONDO and K. NAGASHIMA: *Proceedings of the International Cosmic-Ray Symposium on High Energy Cosmic-Ray Modulation, Tokyo, Japan, 1976*, p. 156; S. SAKAKIBARA, K. FUJIMOTO, Z. FUJII, H. UENO, I. KONDO and K. NAGASHIMA: *Proceedings of the International Cosmic-Ray Symposium on High Energy Cosmic-Ray Modulation, Tokyo, Japan, 1976*, p. 162; S. SAKAKIBARA, K. FUJIMOTO, Z. FUJII, H. UENO, I. KONDO and K. NAGASHIMA: *Proceedings of the International Cosmic-Ray Symposium on High Energy Cosmic-Ray Modulation, Tokyo, Japan, 1976*, p. 316; S. SAKAKIBARA, H. UENO, K. FUJIMOTO, Z. FUJII, I. KONDO and K. NAGASHIMA: *Proceedings of the XVI International Cosmic Ray Conference, Kyoto, 1979*, **4**, 216; S. SAKAKIBARA, H. UENO, K. FUJIMOTO, Z. FUJII, I. KONDO and K. NAGASHIMA: *Proceedings of the International Symposium on Cosmic Ray Modulation in the Heliosphere, Morioka, Japan, 1984*, p. 314.
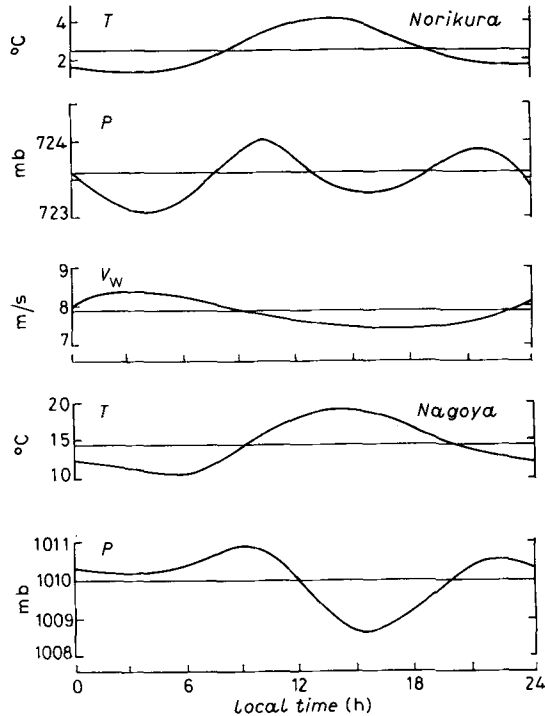
Fig. 1. – Daily variation of atmospheric pressure (P), temperature (T) and wind velocity (V_W) at Mt. Norikura ($h = 2770$ m above sea-level; geographic latitude $\lambda = 36.1°$ N, longitude $\varphi = 137.6°$ E) in 1972 and at Nagoya ($h = 77$ m; $\lambda = 35.2°$ N, $\varphi = 137.0°$ E) in 1965.

intensity variation of cosmic rays due to the change of T_R is less than 0.01% within a day.

The muon telescope consists of seventy-two detectors, each containing a plastic scintillator $(1.0 \times 1.0 \times 0.05)$ m^3 and a five-inch photomultiplier (DuMont 6364) in an iron box with a thickness of 1.6 mm. Counting rate of each detector is about $\sim 1.5 \cdot 10^6$/hour. A detailed description of the telescope was reported elsewhere [10]. We used, for AS-observation, a half of the detectors in upper layer in the early period (August 1970-January 1973), and later we have used those in the lower layer together with those beside the telescope, being propped against T-shaped lead wall located for the absorption of incident cosmic rays from the direction of the other side (cf. fig. 2). In August 1970, an AS-observation was started, which uses four corner trays designated A, B, C and D, each having an area of 4 m^2. Any 3-fold coincidences out of 4 signals from these trays are selected as the air shower events and designated ^3F. The observation of 4-fold coincidence among these trays, called ^4F, was started in May, 1972. Trigger level

[10] Y. SEKIDO, K. NAGASHIMA, I. KONDO, H. UENO, K. FUJIMOTO, Z. FUJII and S. SAKAKIBARA: Report of Cosmic-Ray Research Laboratory, Nagoya Univ., no. 2 (1975).
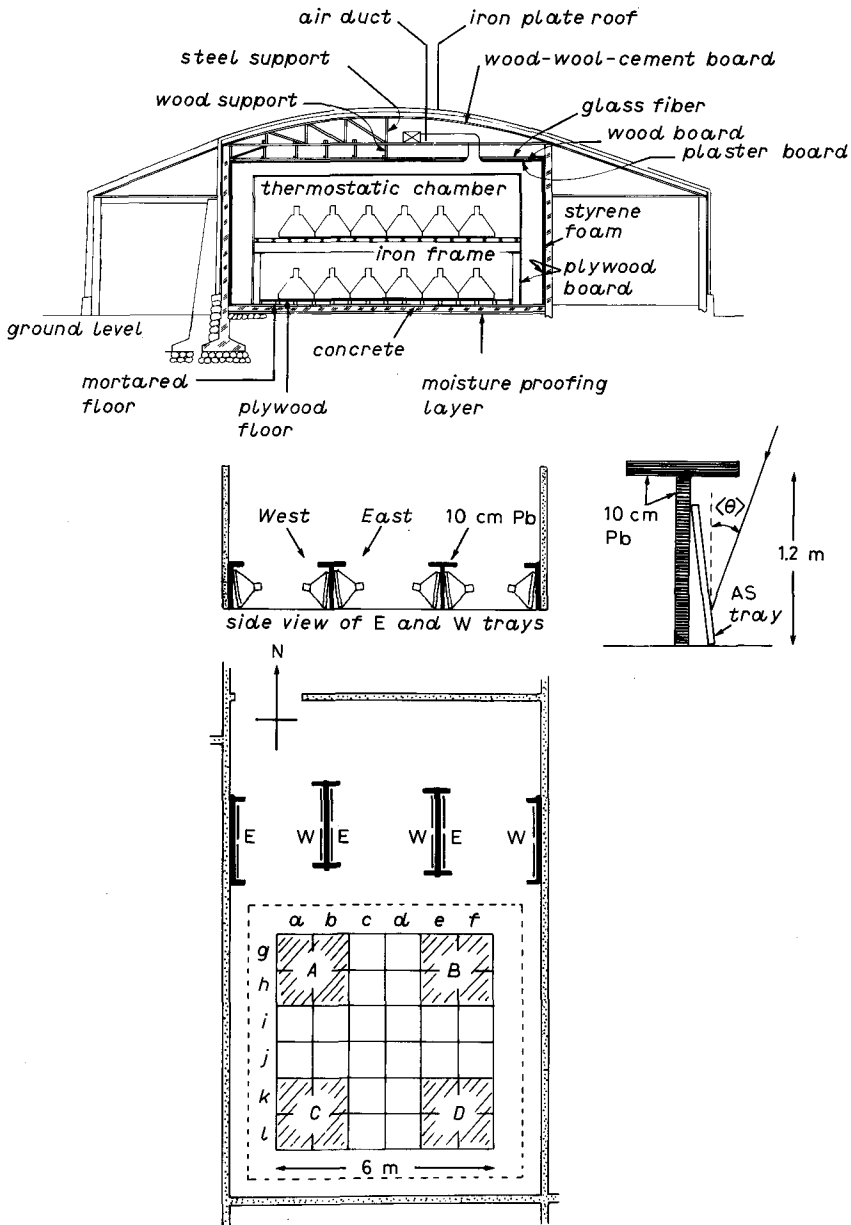
Fig. 2. – Air shower array at Mt. Norikura. A, B, C, D: trays of 4 m² each. a, b, ..., f; g, h, ..., l: trays each consisting of 6 detectors (6 × 1m²) in a row or in a column. E, W: trays, each consisting of 6 slanted detectors (6 × 1m²). Coincidence system of air showers is shown in table I.

TABLE I. – *Components of air showers and their characteristics.*

Component	Count. rate $N \cdot 10^3$/hour	Barometer coefficient β (%/mb)	Temperature coefficient α (%/°C)	Combination of coincidence (*) (cf. fig. 2)
^3F	37	-0.70 ± 0.02	-0.09 ± 0.03	$ABC + BCD + CDA + DAB$
^4F	12	-0.75 ± 0.04	-0.11 ± 0.06	$ABCD$
^{36}F	0.7	-0.76 ± 0.04	-0.11 ± 0.03	$(1 \cdot 2 \cdot 3 \cdot ---- \cdot 35 \cdot 36)$
$^3E; \,^3W$	18	~ -0.70	~ -0.1	$(ac + ad + ae + af)(E; W)$
$^4E; \,^4W$	15	~ -0.70	~ -0.1	$(ace + acf + adf + bdf + $ $+ gik + gil + gjl + hjl)(E; W)$
$^7E; \,^7W$	8	~ -0.75	~ -0.1	$(abcdef + ghijkl)(E; W)$

(*) Numeral: number of 1 m² detector, + signals mixed, product: coincidence.

of each tray is set at ~ 1 particle/4m² and each pulse has a square shape with a time width of 200 ns. Total counting rates of ^3F and ^4F are listed in table I. After February, 1973, the detectors in the upper layer for the AS-observations were switched to the corresponding detectors in the lower layer almost on the floor level, and 12 upper-layer detectors were shifted on the floor beside the telescope to constitute the E- and W-trays as shown in fig. 2. The purpose for this rearrangement is to observe directional air showers. By taking the difference of the directional shower fluxes, one can eliminate direction-independent phenomena, such as the atmospheric effects. The directivity of the showers can be made by the absorption of shower particles by the T-shaped lead wall with 10 cm thickness (cf. fig. 2). According to the selection rule in table I, three pairs of directional shower events (^3E, ^3W; ^4E, ^4W; ^7E, ^7W) are selected from coincidences among signals from the horizontal trays ($a, b, ..., f; g, h, ..., k, l$) and the trays E and $W((6 \times 1)$ m² each) propped against the lead wall (cf. fig. 2). Each of the trays ($a, ..., f$) or ($g, ..., l$) is composed of 6 detectors (1m² each) in a column or in a row in fig. 2. Trigger level of these trays and of the trays E and W is set at ~ 1 particle/tray. Counting rates of these showers are listed in table I. It is noted that each pair of showers such as ^3E and ^3W contains common events of about 25% owing to the incompleteness of the absorption by the lead wall and also to the disorderliness of the direction of individual shower particles caused by the scattering with air nucleus. These events, however, can also be eliminated by taking the difference between ^3E- and ^3W-directional showers. We have been observing also AS events of another kind (^{36}F) since February 1977, which are coincidences of all the signals from 36 horizontal detectors of 1m² each and are produced from primary cosmic rays with high median energy (cf. table I). The purpose of this observation is to determine the energy spectrum of the anisotropy in these regions. Although the counting rate of the shower is

considerably smaller than others, we could determine the spectrum if it is proportional to E or $\sqrt{E}$ as suggested by Linsley and Watson[3] and Fichtel and Linsley[4].

3. – Nature of small air showers.

3˙1. *Local showers.* – Small air showers contain more or less the so-called local air showers in addition to the extensive air showers (EAS). The local showers are supposed to be mainly due to the knock-on electrons and bremsstrahlung photons produced from cosmic-ray muons in the material above the detector such as the roof and wall and also in the air. Primary cosmic rays responsible for these showers are supposed to have a median energy of several hundred GeV and to be subject to various kinds of modulation in the interplanetary magnetic field of the solar system. Therefore, the contamination of the local showers disturbs the observation of sidereal daily variation of galactic origin. In the present observation, as the distance between AS-trays is as short as 4 m, a considerable amount of the local air showers would be contained. There are two experimental methods to estimate the contamination, one is to use the difference between the barometer effects of the two kinds of showers and the other is to use the difference of their density spectra; the density of the local showers is extremely lower than that of EAS and, as will be cleared later, they are supposed to have a narrow band spectrum which can be treated as a Gaussian distribution or the delta-function. Characteristic difference of the density spectrum would be reflected in the dependence of the AS flux (I) on the area (S) of the tray. Figure 3 shows the S-dependences of air showers of twofold (2f) and threefold (3f) coincidences. In the figure, the dependences observed at Nagoya station (77 m above sea level) are also shown in order to demonstrate the difference of the relative contribution of the two kinds of showers at mountain and sea level stations. Solid lines in the figure express, respectively, those theoretically expected from EAS only. The calculation was made by using the size spectrum presented by Greisen[11] and the N-K function[12] for the lateral distribution of electrons. Greater deviations of the observed points from the expected lines at Nagoya than at Mt. Norikura can be regarded as an indication of the increase of the relative contribution of local air showers with the increase of the atmospheric pressure at the station, which is due to the difference of the absorption mean free path of EAS and the parent

---

[11] K. GREISEN: *Progress in Cosmic Ray Physics*, Vol. 3 (North-Holland Publishing Company) 2nd printing, 53 (1965).

[12] J. NISHIMURA and K. KAMATA: *Progr. Theor. Phys.*, 7, 185 (1952); K. KAMATA and J. NISHIMURA: *Suppl. Prog. Theor. Phys.*, 6, 93 (1958).
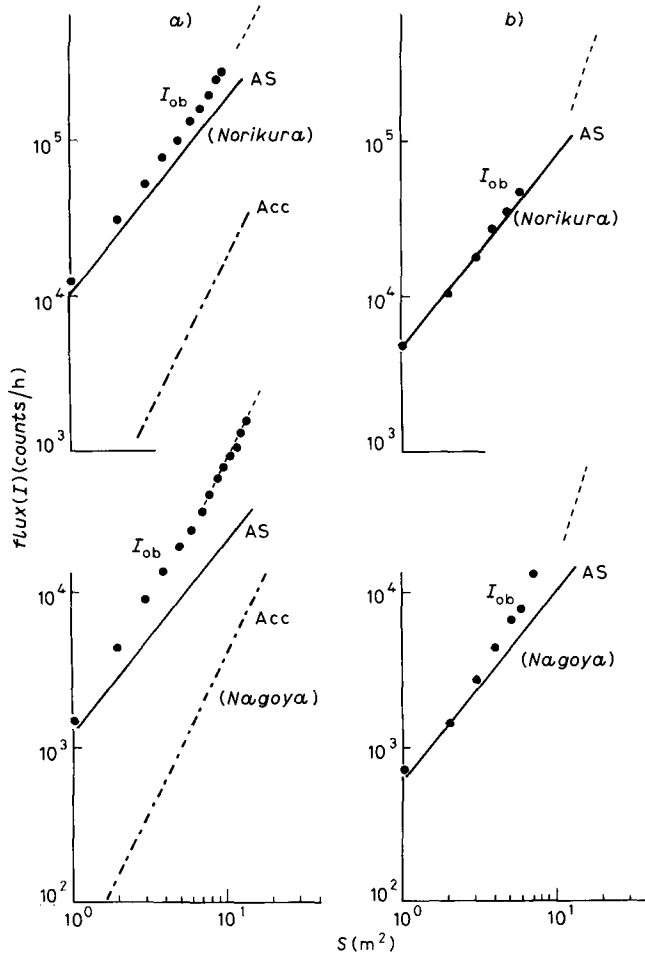
Fig. 3. – Detector-area (S) dependence of twofold (a)) and threefold (b)) air shower flux at Mt. Norikura and Nagoya. Points express the observed flux (I), and solid and chained lines express, respectively, the expected fluxes of EAS and the accidental coincidence. Dashed lines with power exponent of 2 and 3 express, respectively, asymptotic directions of a) 2-fold and b) 3-fold air showers due to the enhancement of local air showers. Altitudes of the stations are, respectively, 2770 m and 77 m above sea level.

muons of the local showers; the reduction rate of EAS flux at Nagoya to that at Mt. Norikura is about 1/9, while that of the muon flux is about 1/2. At Nagoya station, the sequence of the observed point seems to tend asymptotically to a dashed line with a power exponent of 2 for 2f air showers and a power exponent of 3 for 3f air showers. As is well known, this tendency is one of the characteristics of the accidental coincidence among independent pulses from the two or three trays. It is noted however that the calculated accidental coincidence shown by a chained line is far less than the observed value and therefore, it cannot be regarded as the origin. One could explain such a dependence by the

contamination of the local showers. Generally, the flux of air showers can be derived from the differential density spectrum $h(\Delta)\mathrm{d}\Delta$ by the following equation ([11]):

$$\text{(1)} \qquad I = \int_0^\infty h(\Delta)\{1 - \exp[-S\Delta]\}^i \mathrm{d}\Delta \,,$$

where Δ is the density, S is the area of the tray and i expresses the i-fold coincidence among signals from the trays with the same area S. In case of EAS, S-dependence of I can be regarded as being almost independent of i (cf. fig. 3). On the other hand, the local showers could have the above-mentioned dependence if we could assume that Δ is extremely low and its spectrum is expressed by a narrow band such as a Gaussian distribution or the delta-function $\delta(x)$. If we use the delta-function for simplicity, I in eq. (1) can be transformed to

$$\text{(2)} \quad I = \int_0^\infty h_0 \delta(\Delta - \Delta_0)\{1 - \exp[-S\Delta]\}^i \mathrm{d}\Delta = h_0\{1 - \exp[-S\Delta_0]\}^i \approx h_0(\Delta_0 S)^i \,,$$

which shows the i-dependence expected from the observation. With the increase of the height of the observation site, the relative contribution of the muon-initiated showers (*i.e.* local showers) to the observed showers is reduced, and the asymptotic approach of the observed points to the dashed line at Mt. Norikura can be seen only slightly in the 2f AS for large S. Based on these data, it is concluded that ^3F contains the local showers of about 15% at Mt. Norikura. This estimate is also supported by the barometer coefficient of $^3F(-0.70\%/\text{mb})$ greater than usually observed ($\sim -0.8\%/\text{mb}$). As the coefficient of muons is $-0.2 \sim -0.3\%/\text{mb}$, the 15% contamination of the local showers could increase the coefficient to the observed value.

3'2. *Accidental coincidence.* – There are two kinds of accidental coincidence, one is among muons including background noises and the other is between muons and air showers. For example, in case of ^3F, the accidental coincidence is composed of the following kinds of coincidence:

$$\text{(3)} \quad A \cdot B \cdot C + B \cdot C \cdot D + C \cdot D \cdot A + D \cdot A \cdot B + (A\text{-}B) \cdot C + (B\text{-}C) \cdot D + (C\text{-}D) \cdot A \,,$$

where $A, B, \ldots$ express the trays, the symbol ($\cdot$) between them expresses the coincidence of the pulses from the trays and the hyphen ($-$) expresses the 2f shower which triggers the hyphened trays but does not trigger other trays. The flux of such a 2f AS is about $6.8 \cdot 10^4$ counts/hour. The accidental coincidence for ^3F is about 7% which is mainly due to the 2f coincidence between a muon and a 2f AS, while that for ^4F is about several percent which is mainly due to the 2f coincidence between a muon and a 3f AS. We call these coincidences the spurious

air showers. Because of the inclusion of the single muon in its constituent, the spurious shower has the same median energy as the muon's and is subject to the solar modulation characteristic in the low-energy region.

3`3. *Median energy and response function of extensive air showers.* – Median energies (E_m) of primary cosmic rays responsible for the extensive air showers in table I are estimated from the median size N_m of the differential response function $f(N)\,dN$ of the air showers calculated by using the N-K function and Greisen's size spectrum mentioned above. Figure 4 shows $f(N)\,dN$ and $\int_0^N f(N)\,dN$ of ^3F, ^4F and ^{36}F. It is noted that the total flux $\int_0^\infty f(N)\,dN$
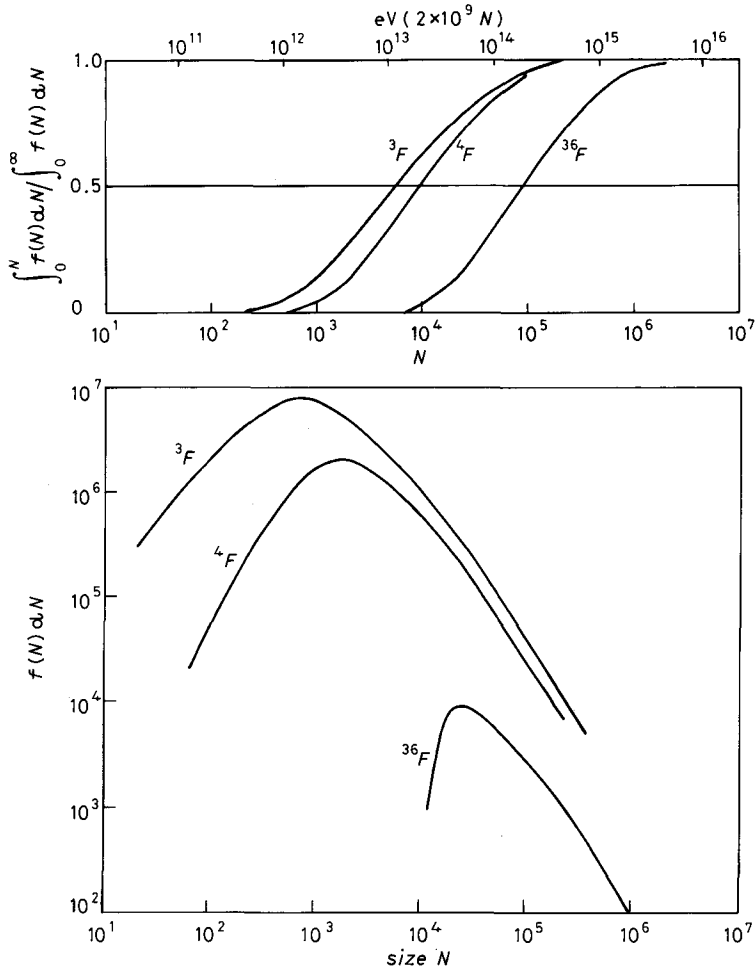
Fig. 4. – Differential and integral response function $f(N)\,dN$ and $\int_0^N f(N)\,dN$ of ^3F, ^4F and ^{36}F.

shows considerably a good agreement with the observation in table I. The median energies and fluxes of directional air showers were not calculated because of a complicate geometrical configuration of the E- or W-tray, but their energies are supposed to be almost comparable with or a little greater than those of ^3F or ^4F, as the pressure coefficients for these showers are nearly equal to or greater than those for ^3F and ^4F (cf. table I).

3`4. *Atmospheric effects.* – Atmospheric pressure and temperature effects of air showers were examined by using the following regression equation:

(4) $$I = I_0 + \beta(P + \varepsilon V_W^2) + \alpha T = I_0 + \beta P + \varepsilon' V_W^2 + \alpha T ,$$

where I, P, T and V_W are, respectively, the daily averages of the AS intensity, the pressure, the temperature and the wind velocity, and I_0, β, α and ε' are their regression coefficients. Although I is influenced by the temperature at all the points in the atmosphere above the detectors, we use, for simplicity, the ground-level temperature at Mt. Norikura or the temperature at an isobar level obtained by radiosonde observation twice a day at Wajima Meteorological Observatory 130 km North of Mt. Norikura. Table II shows the isobar-level dependence of the regression coefficients together with their partial correlation coefficients for ^3F. Data used for the analysis are those in the period of August 1970-June 1973, during which data of the wind velocity were available. As can be seen in the

TABLE II. – *Dependence of daily average intensity (I) of ^3F on the atmospheric temperature at different isobar levels. $I = I_0 + \beta(P + \varepsilon V_W^2) + \alpha T$, P: pressure on the ground, T: temperature at different atmospheric depths, V_W: wind velocity near the ground. Data used for the analysis are those in the period of August, 1970-June, 1973 and their total number is listed under each isobar level.*

Partial correlation coefficients

	723 mb ground	700 mb	600 mb	500 mb	400 mb	100 mb
Isobar level days	272	351	351	351	272	80
$R_{IP \cdot TV_W^2}$	− 0.97	− 0.97	− 0.98	− 0.98	− 0.98	− 0.97
$R_{IT \cdot PV_W^2}$	− 0.43	− 0.55	− 0.58	− 0.58	− 0.48	+ 0.32
$R_{IV_W^2 \cdot PT}$	− 0.57	− 0.52	− 0.50	− 0.47	− 0.47	− 0.26
$R_{PT \cdot IV_W^2}$	− 0.16	− 0.42	− 0.48	− 0.50	− 0.40	+ 0.16

Partial regression coefficients

	723 mb ground	700 mb	600 mb	500 mb	400 mb	100 mb
β (%/mb)	− 0.70	− 0.68	− 0.68	− 0.69	− 0.70	− 0.72
ε (mb/(m/s)^2)	0.007	0.007	0.006	0.006	0.006	0.004
α (%/°C)	− 0.10	− 0.10	− 0.11	− 0.11	− 0.10	+ 0.09

table, the partial correlation coefficient $r_{IT.P}$ shows the maximum at $(500 \div 600)$ mb, indicating that air showers are developed mainly from the region $(100 \div 200)$ g/cm^2 above the ground. It is noted however that even if we use the temperature at the ground, α is not much different from that showing the best partial correlation coefficient. Theoretically, the temperature coefficient is determined by the following equation [13]:

$$\text{(5)} \qquad\qquad \alpha = -100(2\xi - 2 - \zeta)/T \qquad\qquad (\%/°C),$$

where T is the absolute temperature, and ξ and ζ are, respectively, the power exponents of the density spectrum $H(\Delta)$ and the decoherence curve $I(L)$ [11], as

$$\text{(6)} \qquad\qquad H(\Delta) = \int_{\Delta}^{\infty} h(\Delta)\, d\Delta \propto \Delta^{-\xi},$$

$$\text{(7)} \qquad\qquad I(L) \propto L^{-\zeta},$$

where L is the distance between shower trays. From eqs. (6) and (1), we get

$$\text{(8)} \qquad\qquad I \propto S^{\xi} \int_{0}^{\infty} t^{-\xi-1}(1 - \exp[-t])^i \, dt.$$

As the integral in this equation is supposed to be practically convergent, I is proportional to S^{ξ}. We can determine ξ from the S-dependence of 3f AS at Mt.

TABLE III. – *Comparison of atmospheric effects of air showers at several stations.* ξ: *power exponent of the density spectrum* (cf. eq. (6)). ζ: *power exponent of the decoherence curve* (cf. eq. (7)).

	Station	Primary energy (eV)	β (%/mb)	α (%/°C)	ξ	ζ
3F	Mt. Norikura (2770 m)	$\sim 2 \cdot 10^{13}$	-0.70 ± 0.02	-0.09 ± 0.03	< 1.2	$0.1 \sim 0.2$
Gombosi et al. [6]	Peak Musala (2925 m)	$6 \cdot 10^{13}$	-0.68 ± 0.004	-0.21 ± 0.004		
Daudin and Daudin [13]	Pic-du-Midi (2860 m)	$(3 \sim 6) \cdot 10^{14}$	-0.76 ± 0.01	-0.11	1.35	~ 0.3
Efimov et al. [14]	Yakutsk (sea level)	$\sim 10^{14}$	-0.75 ± 0.015	-0.21		
Hodoson [15]	Manchester (sea level)	$5 \cdot 10^{14}$		-0.38 ± 0.11	1.445	~ 0.1

[13] A. DAUDIN and J. DAUDIN: *J. Physique et le Radium*, **14**, 169 (1953).
[14] N. N. EFIMOV, D. D. KRASILNIKOV, S. I. NIKOLSKY and F. K. SHAMSUTDLNOVA: *Canad. J. Phys.*, **46**, S84 (1968).
[15] A. L. HODSON: *Proc. Phys. Soc. A*, **64**, 1061 (1951).

Norikura in fig. 3 because the slope for small S is not much influenced by the contamination of local air showers. The value of ζ in eq. (7) also was estimated experimentally. These three parameters (α, ξ, ζ) are shown in table III and seem to satisfy eq. (5) approximately. In the table, we show also those data obtained by other groups, for reference. The differences among α's could be regarded as being due to the difference of the values of ξ and ζ for each air shower observation.

Air shower intensity is also influenced indirectly by wind velocity (V_W) owing to the wind effect to the pressure. We assumed that the effect is proportional to the square of the velocity, as shown in eq. (4). On the other hand, the wind effect at Mt. Norikura was studied also by Kawasaki[16]. He derived the following regression equation from the correlation analysis between neutron intensity (I_N) and the wind velocity.

$$(9) \qquad I_N = I_{N,0} + \beta_N (P + \varepsilon_{N1} V_W + \varepsilon_{N2} V_W^2),$$

where

$$(10) \qquad \varepsilon_{N1} = 0.089 \, \text{mb/(m/s)}, \qquad \varepsilon_{N2} = 0.0019 \, \text{mb/(m/s)}^2.$$

Although two regression equations (4) and (9) are different in form with respect to V_W, they give almost the same effect in strong wind region. It is noted that V_W has not been observed since 1974, owing to the heavy snow fall on the anemometer every winter and cannot be used in the following analysis.

The most dominant atmospheric effect is due to the pressure variation. For the determination of β, the temperature and velocity effects need not to be taken into account, as the regression coefficients α and ε are very small (cf. table II). In table I, we have shown the barometer coefficients for various kinds of air showers obtained by neglecting other atmospheric effects. The coefficient for ^3F shows a smaller value than others. This is due to the contamination of the muon-initiated showers (i.e. local air showers) as pointed out previously.

4. – Daily variations.

4‘1. *Analysis.* – The present method of analysis to obtain the galactic anisotropy is different from that used for the previous reports[5,8]. The previous analyses were made according to the following procedure: 1) the observed hourly intensity I was corrected for the pressure effect using the barometer coefficient listed in table I but not corrected for the atmospheric temperature effect, 2) the diurnal and semidiurnal harmonic vectors $(\boldsymbol{a}^1(d), \boldsymbol{a}^2(d))$ were obtained every day,

[16] S. KAWASAKI: *Sci. Papers Inst. Phys. Chem. Res. (Japan)*, **66**, 25 (1972).

using hourly data, 3) the monthly averages of $a^1(d)$ and $a^2(d)$ were obtained by eliminating those vectors with their amplitude ($|a^1(d)|$, $|a^2(d)|$) three times greater than their statistical errors and 4) using the monthly averages, the solar, sidereal and antisidereal vectors were obtained. By this method, we could derive the statistically significant sidereal diurnal and semidiurnal variations of ^3F and ^4F and could regard them, with the aid of the directional air shower observation, as being due to the galactic anisotropies. In the present paper, we use an analysis method different from the previous one in the following points. 1) Firstly, we change the method of the barometer correction for the following reason. We have used the self-recording Fortin barometer called «Agari»-type which measures the change of ohmic resistance of thin platina string vertically stretched in the centre of the barometer tube. Because of the friction (i.e. surface tension) of the mercury against the string, the change of the resistance and therefore that of the observed pressure lags behind the real pressure change. This lag time (τ_P) is supposed to increase with the oxidation of mercury as time goes on and therefore to be subject to a long term drift. We purified the mercury twice within about 10 years and finally we gave up to use the barometer and have switched to a new type barometer called «Digiquartz Pressure Transducer, Model 215-AS» from October 1982. After careful comparison of these two types of barometer at Nagoya Muon Observatory with the standard one at Nagoya Meteorological Observatory in the period of April 22-August 20, 1981, we found the lag time of 11 minutes and the attenuation factor (0.94) of the semidiurnal amplitude [17]. Individual barometer is supposed to have its proper lag time. Therefore, we examined also the lag time of the barometer, having been set at Mt. Norikura, by comparing the solar second harmonic vectors of the pressure observed, respectively, by the barometers of two types. Figure 5
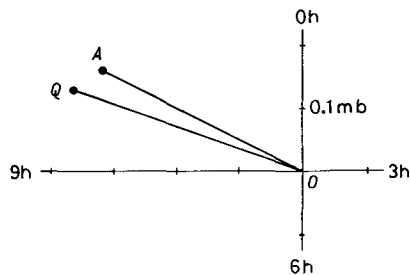
Fig. 5. – Solar semidiurnal harmonic vector of atmospheric pressure at Mt. Norikura. $\overline{OA}$: average obtained by old-type barometer (1973-1982). $\overline{OQ}$: average obtained by new-type barometer (1983-1987). $OA/OQ = 0.92$, $\widehat{AOQ} = 13.6\,\text{min}$.

[17] S. SAKAKIBARA, T. YAMADA, H. SATAKE, Z. FUJII and K. MURAKAMI: *Proceedings of the Cosmic-Ray Research Laboratory of Nagoya University*, **26**, 13 (1983) (in Japanese).

shows the average vectors in the two periods. The phase lag (Δt) of the vector is 13.6 minutes and the attenuation factor (f_a) of the amplitude is 0.92. These values show fairly a good agreement with those obtained at Nagoya station, mentioned in the above. We use these data for the barometer correction of hourly intensity $I_{ob}(t)$ in the period prior to October 1982, as

$$(11) \quad I_c(t) = I_{ob}(t) + (\beta/f_a) P(t + \Delta t) \approx I_{ob}(t) + (\beta/f_a)\left\{P(t) + \frac{dP}{dt}\Delta t\right\} \approx$$

$$\approx I_{ob}(t) + (\beta/f_a)\left[P(t) + \{P(t + 1\,\mathrm{h}) - P(t)\}\frac{\Delta t}{1\,\mathrm{h}}\right],$$

in which β is the coefficient listed in table I. 2) After the pressure correction, we take the deviation of hourly data from the 24-hour running average in order to eliminate longer term variation than 24 hours, such as due to the day-to-day variation of the temperature and the instrumental deterioration. The effect of the daily temperature variation is different from that of the day-to-day variation and will be taken into account in the following analysis. 3) We assume the following equation and determine unknown parameters in the equation by the least-squares method

$$(12) \quad \Delta I(d, t) = \alpha \Delta T(d, t - \tau) + \sum_{m=0}^{5}\left\{A^m(\mathrm{SO})\cos\frac{2\pi m}{24}t + B^m(\mathrm{SO})\sin\frac{2\pi m}{24}t\right\} +$$

$$+ \sum_{m=1}^{3}\left\{A^m(\mathrm{SI})\cos\frac{2\pi m}{24}t_{\mathrm{SI}} + B^m(\mathrm{SI})\sin\frac{2\pi m}{24}t_{\mathrm{SI}}\right\} +$$

$$+ \sum_{m=1}^{2}\left\{A^m(\mathrm{ATS})\cos\frac{2\pi m}{24}t_{\mathrm{ATS}} + B^m(\mathrm{ATS})\sin\frac{2\pi m}{24}t_{\mathrm{ATS}}\right\} + A^1(\mathrm{SI}_2)\cos\frac{2\pi}{24}t_{\mathrm{SI}_2} +$$

$$+ B^1(\mathrm{SI}_2)\sin\frac{2\pi}{24}t_{\mathrm{SI}_2} + A^1(\mathrm{ATS}_2)\cos\frac{2\pi}{24}t_{\mathrm{ATS}_2} + B^1(\mathrm{ATS}_2)\sin\frac{2\pi}{24}t_{\mathrm{ATS}_2} +$$

$$+ A^2(\mathrm{SI}_{1/2})\cos\frac{2\times 2\pi}{24}t_{\mathrm{SI}_{1/2}} + B^2(\mathrm{SI}_{1/2})\sin\frac{2\times 2\pi}{24}t_{\mathrm{SI}_{1/2}} +$$

$$+ A^2(\mathrm{ATS}_{1/2})\cos\frac{2\times 2\pi}{24}t_{\mathrm{ATS}_{1/2}} + B^2(\mathrm{ATS}_{1/2})\sin\frac{2\times 2\pi}{24}t_{\mathrm{ATS}_{1/2}}$$

$$\text{for } t = 1, 2, ..., 24\,\text{hour}; \; d = 1, 2, ..., 365\,\text{day},$$

where ΔI and ΔT are, respectively, the hourly deviations of I_c and T (the ground-level temperature) from the 24-hour running averages, and (d, t) expresses the solar local time (t hour) on the d-th day counted from the autumnal equinox. By introducing the lag time ($\tau > 0$) into ΔT as a parameter, we try to obtain the temperature coefficient (α) due to the temperature variation in the upper atmosphere, where air showers are mainly produced. Terms with the symbol

(SO) express the harmonics of solar daily variation, which express not only those of space origin such as due to the Compton-Getting effect arising from the Earth's revolution around the Sun but also those of the unidentified atmospheric origin such as due to the wind effect. On the other hand, the terms with the symbol (SI) express the harmonics of sidereal daily variation and t_{SI} expresses the sidereal time. We take into account the first to third harmonics in the present analysis. Terms with other symbols can be produced by the annual modulation of solar diurnal ($m = 1$) and semidiurnal ($m = 2$) variations. If the solar m-th harmonic variation with the frequency of 365m cycle/year is modulated by a variation with the frequency k cycle/year, we can observe additional two kinds of variation with sideband frequencies $m (365 + k/m)$ and $m(365 - k/m)$ cycle/year. We define day and hour by 1 year/$(365 \pm k/m)$ and 1 day/24, and express the hourly time as $t_{SI_{k/m}}$ for the plus sign and $t_{ATS_{k/m}}$ for the negative sign. We normalize these times at the autumnal equinox and call them the extended sidereal and antisidereal times [18]. Sidereal and antisidereal times correspond to $k = m$ and, in this case, we delete the subscript $k/m (= 1/1$ or $2/2)$ from the symbols $SI_{k/m}$ and $ATS_{k/m}$. It is emphasized here that these variations can be also produced by the heliomagnetic modulation of sidereal m-th harmonic variation (366 m cycle/year) of galactic origin. For example, if the sidereal diurnal variation ($m = 1$) is subject to the annual variation (1 cycle/year), it produces the variations of $(366 + 1)$ and $(366 - 1)$ cycle/year, which correspond, respectively, to the variations of SI_2 and SO. Therefore, the observation of these variations provides information on the annual modulation of the diurnal and semidiurnal variations not only of the atmospheric origin but also of solar and galactic origins. In the equation, the wind effect mentioned previously cannot be taken into account explicitly owing to the lack of data for all the periods. The effect, if exists, would be contained in the harmonic terms in the equation. Presetting several value of τ in eq. (12), we have determined the harmonic coefficients (A^m's, B^m's) and α by the least-squares method. It was found by the analysis that the temperature coefficient α is negligibly small as can be seen in table IV. The small value of α as compared with that of the day-to-day variation in table II would be attributed to the different change of the atmospheric distribution of temperature. In case of the day-to-day variation, the temperature in the upper

TABLE IV. – *Temperature coefficient (α) for daily variation of air showers (^3F). τ: lag time of temperature (cf. eq. (12)).*

τ	0 h	1 h	2 h	3 h
α (%/°C)	0.0016	0.0016	− 0.0009	− 0.0037
$\Delta\alpha$	± 0.2809	± 0.2809	± 0.2810	± 0.2810

[18] K. NAGASHIMA and H. UENO: *Rep. Ionos. Space Res., Japan*, **25**, 212 (1971).

atmosphere is well correlated to the ground-level temperature, whereas in case of the daily variation, the both temperatures would not always be well correlated to each other, thus producing the negligible temperature effect. Similar result can be inferred from the air shower observation at Baxan by Alexeenko *et al.* [7]. They have succeeded to observe the solar diurnal variation due to C-G effect arising from the Earth's revolution around the Sun. In their analysis, however, the correction for the temperature effect has not been made. This seems to support the present result of analysis that the regression coefficient (α) is very small in case of the daily temperature variation. In the following analysis, we decide to delete the temperature term from eq. (12) in order to prevent the loss of air shower data due to the failure of the temperature observation caused by the heavy snow fall in Winter.

4`2. *Average harmonic vectors*. – In the present analysis, we use those data in the period after 1973 and omit other data in 1970-1972 due to the difficulty to use them owing to the difference of the recording system in those days. The results in those periods should be referred to the previous papers [5,9]. We analyse these data every year. Figure 6 shows the yearly averaged first ($m = 1$) and second ($m = 2$) harmonic vectors ${}^{i}F^{m}(H)$'s of the i-fold air showers in the t_{H}-time coordinate system. Errors for these vectors are derived from the dispersion of the yearly vectors. These results are also listed in table V. We list also the corresponding vectors of P and T in table VI for future reference. Note that the corresponding vectors of the room temperature (T_{R}) are not shown in the table

TABLE V. – ${}^{3}F^{m}(H)$ and ${}^{4}F^{m}(H)$. *Solar, extended-sidereal and extended-antisidereal* 1st ($m = 1$) *and* 2nd ($m = 2$) *harmonic vectors of air showers* (${}^{3}F^{m}$, ${}^{4}F^{m}$) *in the period* 1973-1987. *Errors are estimated from the dispersion of yearly vectors. Figures in parentheses express the ratio of the amplitude to the error. If the ratio is less than* 1.0, *the error of the phase is not shown.*

	1st ($m = 1$)			2nd ($m = 2$)		
	H	amplitude ($\cdot 10^{-4}\%$)	phase (h)	H	amplitude ($\cdot 10^{-4}\%$)	phase (h)
${}^{3}F^{m}$	SI$_{2}$	152 ± 40 (3.8)	17.2 ± 0.9	SI	180 ± 25 (7.3)	6.3 ± 0.3
	SI	602 ± 27 (22.0)	0.8 ± 0.3	SI$_{1/2}$	66 ± 34 (1.9)	11.6 ± 0.7
	SO	479 ± 29 (16.6)	12.9 ± 0.4	SO	63 ± 26 (2.4)	10.2 ± 0.9
	ATS	119 ± 44 (2.7)	7.0 ± 1.2	ATS$_{1/2}$	12 ± 26 (0.5)	0.5
	ATS$_{2}$	142 ± 38 (3.8)	13.2 ± 0.7	ATS	38 ± 26 (1.5)	3.2 ± 1.2
${}^{4}F^{m}$	SI$_{2}$	109 ± 54 (2.0)	17.9 ± 2.1	SI	205 ± 32 (6.4)	5.7 ± 0.4
	SI	664 ± 34 (19.4)	1.2 ± 0.4	SI$_{1/2}$	76 ± 43 (1.7)	0.7 ± 0.9
	SO	415 ± 39 (10.5)	12.5 ± 0.6	SO	164 ± 40 (4.1)	9.6 ± 0.5
	ATS	178 ± 49 (3.7)	8.3 ± 1.0	ATS$_{1/2}$	45 ± 40 (1.1)	4.3 ± 1.4
	ATS$_{2}$	128 ± 35 (3.7)	12.3 ± 1.0	ATS	9 ± 39 (0.2)	9.9
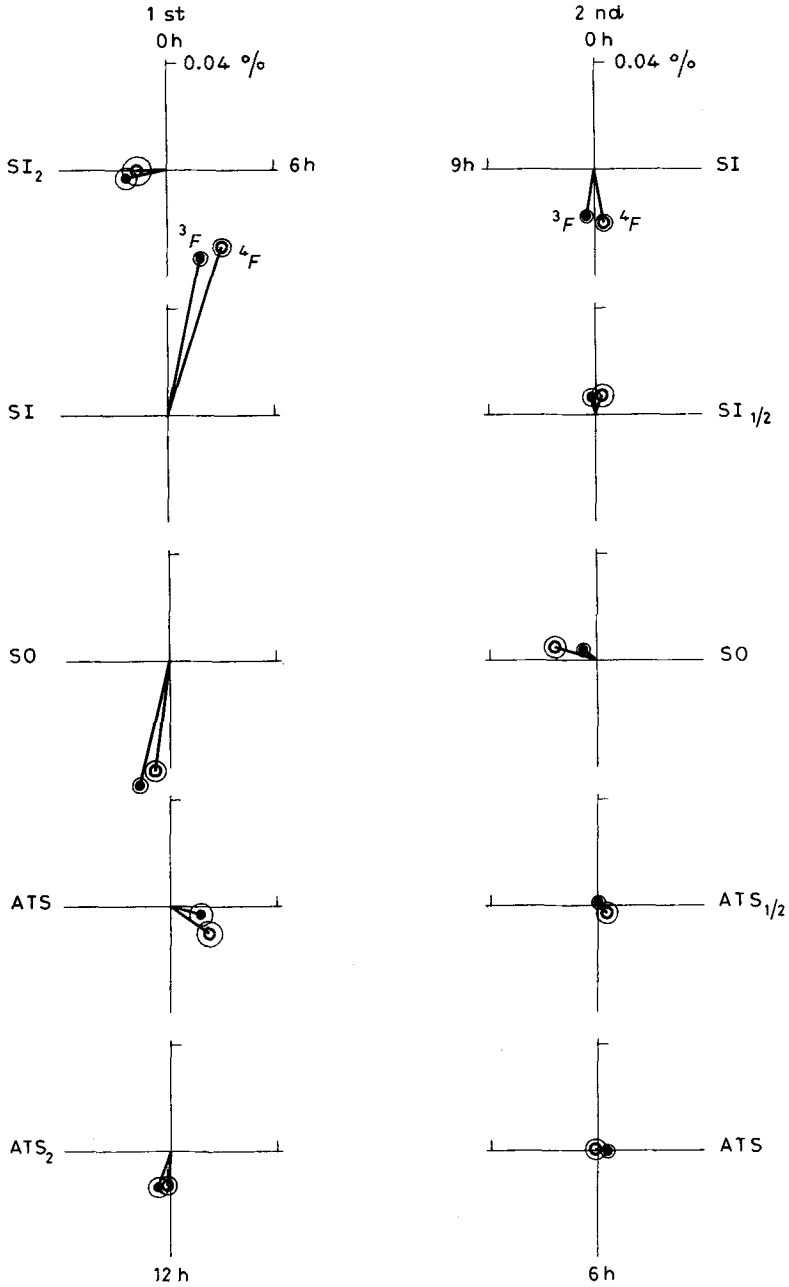
Fig. 6. – $^3F^m(H)$ and $^4F^m(H)$. Solar, extended-sidereal and extended-antisidereal 1st ($m = 1$) and 2nd ($m = 2$) harmonic vectors of ^3F and ^4F in the period 1973-1987. Errors shown by circles are estimated from the dispersion of yearly vectors. ● $^3F^m$, ○ $^4F^m$.

TABLE VI. – $P^m(H)$ *and* $T^m(H)$. *The harmonic vectors of pressure (P) and atmospheric temperature (T) corresponding to those vectors in table V.*

	st $(m = 1)$			2nd $(m = 2)$		
	H	amplitude	phase (h)	H	amplitude	phase (h)
P^m	SI_2	10 ± 5	18.5 ± 2.2	SI	23 ± 3	0.0 ± 0.3
$(\cdot 10^{-3}\,\text{mb})$	SI	31 ± 7	7.4 ± 0.8	$SI_{1/2}$	41 ± 3	10.3 ± 0.2
	SO	147 ± 5	16.5 ± 0.2	SO	367 ± 5	9.8 ± 0.0
	ATS	24 ± 7	0.6 ± 1.0	$ATS_{1/2}$	66 ± 2	4.8 ± 0.1
	ATS_2	12 ± 6	7.8 ± 1.7	ATS	15 ± 2	11.2 ± 0.2
T^m	SI_2	20 ± 2	14.9 ± 0.4	SI	9 ± 1	1.9 ± 0.2
$(\cdot 10^{-2}\,°\text{C})$	SI	37 ± 2	7.6 ± 0.3	$SI_{1/2}$	5 ± 1	9.7 ± 0.2
	SO	136 ± 2	13.6 ± 0.1	SO	33 ± 1	0.7 ± 0.0
	ATS	24 ± 2	17.8 ± 0.4	$ATS_{1/2}$	12 ± 1	11.6 ± 0.2
	ATS_2	8 ± 2	11.0 ± 0.8	ATS	6 ± 1	11.5 ± 0.2

as they are extremely small ($< 0.01\,°C$) and would not disturb the observation of the sidereal anisotropy.

As can be seen in fig. 6 and table V, the general characteristics of the variations of air showers are as follows:

1) The vectors $^3F^m(H)$'s coincide fairly well with the corresponding vectors $^4F^m(H)$'s. The coincidence indicates the reliability of the observation, although ^3F and ^4F are not mutually independent perfectly because the latter is included in ^3F.

2) Some of these vectors are statistically significant in some degree.

In order to determine the origin of these significant vectors in the above, we examine, in what follows, the time variation of the directional air shower flux. As mentioned previously, the directional air showers (East- and West-components) have been observed in order to eliminate the atmospheric influence from the variations by taking their difference $(E - W)$. Figure 7 illustrates how the diurnal and semidiurnal harmonic vectors of $(E - W)$ reflect the cosmic-ray anisotropy in space. $^iE^m$ and $^iW^m$ express, respectively, the m-th harmonic vectors of i-fold directional air showers observed by E- and W-telescopes. These vectors in fig. 7 are respectively composed of two terms, one is $^iC^m$ due to the atmospheric effect or the malfunction of the telescopes and common to both telescopes, and the other is $^iE^{*m}$ or $^iW^{*m}$ due to the cosmic-ray anisotropy indicated by an arrow in the figure. $\langle\psi\rangle$ is the median zenith angle of the directional air showers, which is dependent on the zenith angle distribution of the showers and also on the geometrical configuration of the tray propped against the lead absorber (cf. fig. 2). (Note that if cosmic rays are subject to the geomagnetic deflection, $^iE^{*m}$ and $^iW^{*m}$ rotate counterclockwise by the deflection
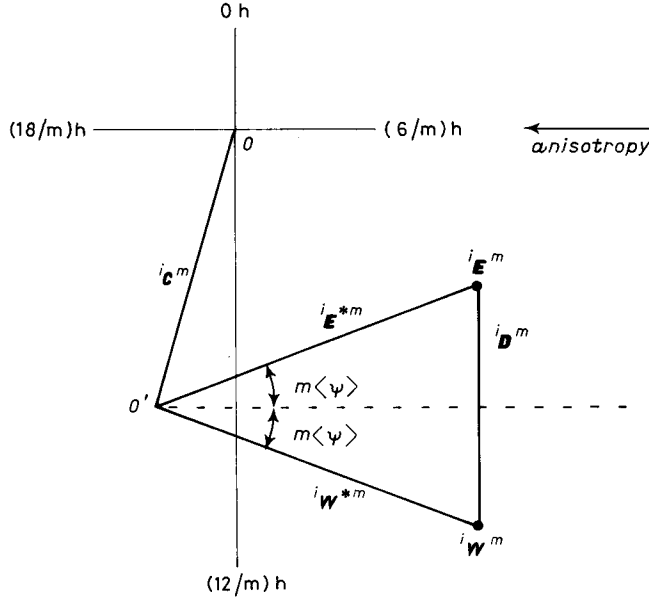
Fig. 7. – Schematic representation of the m-th harmonic vectors ${}^{i}E^{m}$ and ${}^{i}W^{m}$ of directional i-fold air showers produced from a cosmic-ray anisotropy in space. $\rightarrow$: direction of anisotropy. ${}^{i}E^{*m}/{}^{i}W^{*m}$: the m-th harmonic vector of directional (E/W) i-fold air showers, produced from the anisotropy. $\langle\psi\rangle$: mean zenith angle of the directional air showers. ${}^{i}C^{m}$: common vector due to the atmospheric effect. ${}^{i}E^{m}/{}^{i}W^{m}$: resultant of ${}^{i}E^{*m}/{}^{i}W^{*m}$ and ${}^{i}C^{m}$. ${}^{i}D^{m} = {}^{i}E^{m} - {}^{i}W^{m}$.

angle). The direction of the anisotropy $({}^{i}\phi^{m})$ can be obtained by the clockwise rotation of the difference vector $({}^{i}E^{m} - {}^{i}W^{m})$ by the right angle, even without knowing the partition of the vectors ${}^{i}C^{m}$, ${}^{i}E^{*m}$ and ${}^{i}W^{*m}$. If $\langle\psi\rangle$ is given, ${}^{i}C^{m}$, ${}^{i}E^{*m}$ and ${}^{i}W^{*m}$ also can be determined as

$$(13) \qquad |{}^{i}E^{*m}| = \frac{|{}^{i}D^{m}|}{2}\operatorname{cosec}(m\langle\psi\rangle), \qquad\qquad \text{for } m = 1, 2,$$

where

$$(14) \qquad {}^{i}D^{m} = {}^{i}E^{m} - {}^{i}W^{m}.$$

The origin (O') of ${}^{i}E^{*m}$ and ${}^{i}W^{*m}$ is determined as indicated in the figure and $\overrightarrow{OO'}$ expresses ${}^{i}C^{m}$. $\langle\psi\rangle$ can be estimated experimentally by the following equation if the solar first harmonic vector $({}^{i}D^{1}(\text{SO}))$ is produced only from the C-G effect mentioned previously and does not contain any contamination due to other anisotropies:

$$(15) \qquad \langle\psi\rangle = \arcsin\left\{\frac{|{}^{i}D^{1}(\text{SO})|}{2G_{e}}\right\},$$

$$(16) \qquad G_e = (\gamma_p + 2)\left(\frac{\xi v}{c}\right)\cos\lambda,$$

where G_e is the amplitude of $\boldsymbol{G_e}$ due to C-G effect, observable with the omnidirectional air shower array, c is the light velocity, γ_p is the power exponent (2.7) of the differential rigidity spectrum of cosmic-rays, v is the velocity of the Earth's revolution, the term ξv expresses the yearly average of the projection of $\boldsymbol{v}$ to the equatorial plane and λ is the geographic latitude of the observation site. We define a vector ${}^i\boldsymbol{R}^m$ having the magnitude given by eq. (13) and the above-mentioned phase ${}^i\phi^m$, and call it the space-originated vector. ${}^i\boldsymbol{R}^m$ can be directly compared with the corresponding vector $({}^i\boldsymbol{F}^m)$ obtained by the omnidirectional air shower observation. The above treatment to derive the vector due to the anisotropy can be applied to any harmonic vector such as solar, extended sidereal and antisidereal variations. If ${}^i\boldsymbol{E}^m$ and ${}^i\boldsymbol{W}^m$ do not show any difference from each other, we cannot confirm the existence of cosmic-ray anisotropy responsible for these vectors.

Figure 8 shows the harmonic vectors $({}^3\boldsymbol{E}^m(H)$ and ${}^3\boldsymbol{W}^m(H);\ m=1,2)$ of the directional air showers in the periods 1975-1978 and 1980-1987. We could not

TABLE VII. – $^3\boldsymbol{E}^m(H)$, $^3\boldsymbol{W}^m(H)$ and $^3\boldsymbol{D}^m(H)$. Solar, extended-sidereal and extended-antisidereal harmonic vectors $(m=1,2)$ of directinal air showers $(^3\boldsymbol{E}^m,\ ^3\boldsymbol{W}^m)$ and their differences $(^3\boldsymbol{D}^m = {}^3\boldsymbol{E}^m - {}^3\boldsymbol{W}^m)$ in the period 1975-78 and 1980-87. Errors are estimated from the dispersion of yearly vectors. Figures in parentheses express the ratio of the amplitude to the error. If the ratio is less than 1.0, the error of the phase is not shown.

	1st ($m=1$)			2nd ($m=2$)		
	H	amplitude ($\cdot\,10^{-4}\%$)	phase (h)	H	amplitude ($\cdot\,10^{-4}\%$)	phase (h)
$^3E^m$	SI$_2$	$154 \pm 53\,(\ 2.9)$	17.2 ± 1.2	SI	$211 \pm 42\,(5.1)$	4.7 ± 0.3
	SI	$629 \pm 48\,(13.2)$	0.2 ± 0.4	SI$_{1/2}$	$100 \pm 42\,(2.4)$	0.7 ± 0.5
	SO	$308 \pm 44\,(\ 7.0)$	12.8 ± 0.9	SO	$58 \pm 28\,(2.1)$	9.7 ± 1.1
	ATS	$146 \pm 57\,(\ 2.6)$	8.8 ± 1.4	ATS$_{1/2}$	$9 \pm 34\,(0.3)$	0
	ATS$_2$	$96 \pm 56\,(\ 1.7)$	16.0 ± 2.1	ATS	$38 \pm 26\,(1.5)$	3.2 ± 1.2
$^3W^m$	SI$_2$	$173 \pm 63\,(\ 2.7)$	16.5 ± 1.0	SI	$192 \pm 41\,(4.6)$	7.7 ± 0.4
	SI	$679 \pm 47\,(14.6)$	1.5 ± 0.3	SI$_{1/2}$	$82 \pm 34\,(2.4)$	11.5 ± 0.8
	SO	$458 \pm 52\,(\ 8.8)$	12.7 ± 0.5	SO	$8 \pm 51\,(0.2)$	4.9
	ATS	$197 \pm 54\,(\ 3.7)$	8.4 ± 1.0	ATS$_{1/2}$	$21 \pm 43\,(0.5)$	11.0
	ATS$_2$	$59 \pm 50\,(\ 1.2)$	11.2 ± 2.5	ATS	$57 \pm 32\,(1.7)$	3.7 ± 1.1
$^3D^m$	SI$_2$	$34 \pm 34\,(1.0)$	1.1 ± 1.6	SI	$282 \pm 40\,(7.1)$	3.3 ± 0.3
	SI	$232 \pm 51\,(4.6)$	18.0 ± 0.7	SI$_{1/2}$	$58 \pm 29\,(2.0)$	2.5 ± 1.2
	SO	$151 \pm 30\,(5.0)$	0.5 ± 1.1	SO	$65 \pm 44\,(1.5)$	9.8 ± 1.0
	ATS	$54 \pm 44\,(1.2)$	19.2 ± 2.4	ATS$_{1/2}$	$14 \pm 39\,(0.4)$	4.3
	ATS$_2$	$97 \pm 47\,(2.0)$	18.4 ± 1.8	ATS	$59 \pm 38\,(1.6)$	8.4 ± 0.9
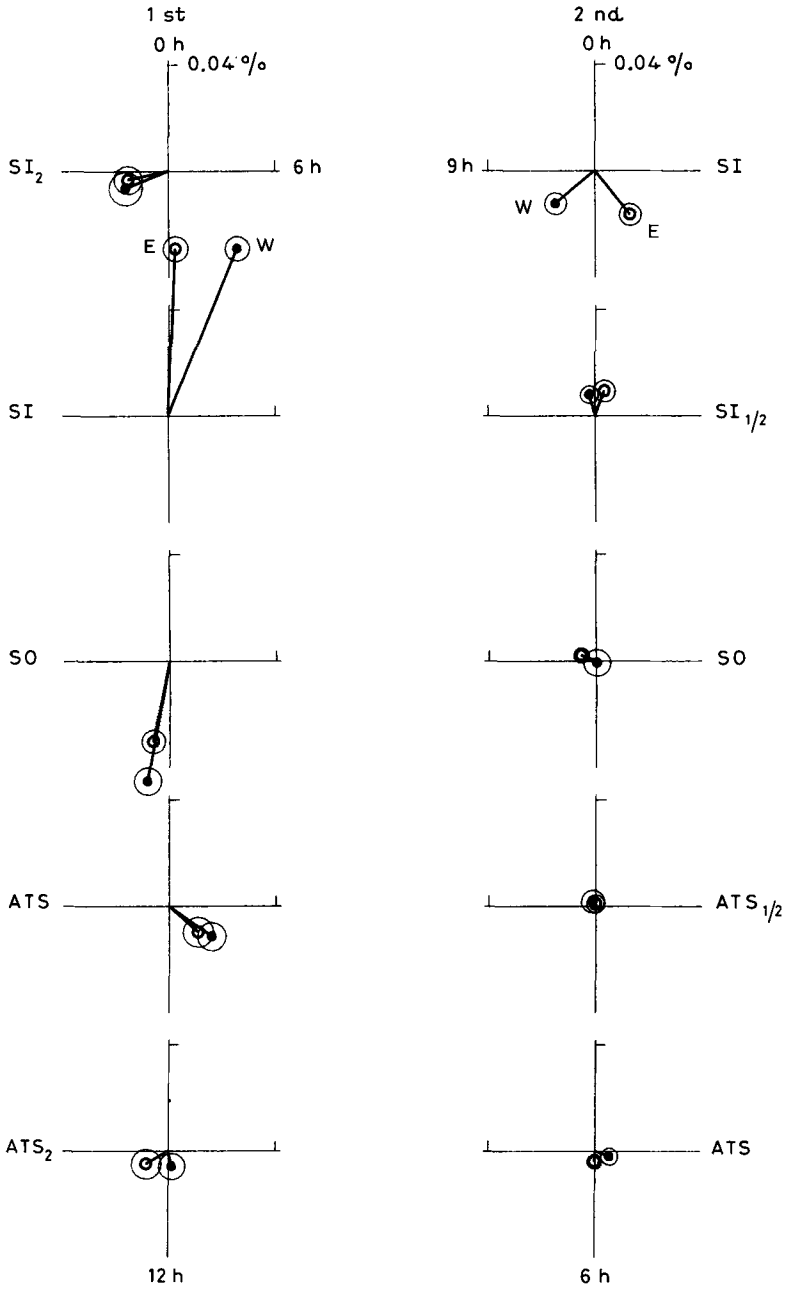
Fig. 8. – $^3E^m(H)$ and $^3W^m(H)$. Solar, extended-sidereal and extended-antisidereal harmonic vectors of directional air showers in the periods 1975-78 and 1980-87. Errors shown by circles are estimated from the dispersion of yearly vectors. ○ $^3E^m$, ● $^3W^m$.

obtain the result in 1979 owing to the malfunction of the directional telescope for a long period of time. The errors attached to the vectors were derived from the dispersion of yearly vectors. These vectors are also summarized in table VII. Except for the sidereal 1st and 2nd harmonics, one cannot find any clearly significant difference between $^3E^m$ and $^3W^m (m = 1, 2)$. We are discouraged more or less at this stage by the fact that $^3E^1(\text{SO})$ and $^3W^1(\text{SO})$ necessary for the estimation of $\langle \psi \rangle$ in eq. (15) also do not show a clear difference from each other, although the direction of their difference $^3D^1$ coincides approximately with the phase (0 hour solar local time) expected from that (6 hour) of the anisotropy due to C-G effect. Fortunately, however, the error can be much reduced if we make $^3D^1(\text{SO})$ every year and derive the error from the dispersion of yearly difference vectors. As can be seen in fig. 9 and table VII, the averaged $^3D^1(\text{SO})$ is 5.0 times greater than the error thus obtained and could be regarded as statistically significant. The reduction of the error by the present method implies that the large error attached to $^3E^1$ and $^3W^1$ is due to large year-to-year fluctuation of common vectors involved in $^3E^1$ and $^3W^1$. Such an inference can be confirmed by the dispersion of the yearly plot of $^3E^1$, $^3W^1$ and $^3D^1$ as shown in fig. 10. It is noteworthy here that the error (0.0030%) of $^3D^1(\text{SO})$ obtained by the present analysis is almost comparable with the error (0.0035%) derived from the counting rate of the directional air showers. This implies that the air shower observation has been operated properly and the present method to take the difference of vectors makes it possible to determine the anisotropy within the statistical error without any disturbance as far as the anisotropy in question is stationary through years. The anisotropy due to the Compton-Getting effect arising from the Earth's revolution is the most typical example for this. As $^3D^1(\text{SO})$ is statistically significant and also as its phase coincides with the direction of zero hour within statistical error, we could regard this vector as being mainly due to the C-G effect in question. It is noted, however, that the phase slightly advances from zero hour. We could regard this advancement as being due to the contamination of the spurious 3-fold air showers produced by the accidental coincidence between one single muon and one 2-fold air shower, as pointed out previously. Owing to the inclusion of the single muon in its constituents, the spurious shower has the same median energy as the muon's and is subject to the solar modulation characteristic in the low-energy region. Therefore, $^3D^1(\text{SO})$ contains the information of solar diurnal variation of muons represented by $V^1(\text{SO})$ observed by the vertical muon telescope at Mt. Norikura. As $V^1(\text{SO})$ has a phase 13.0 hour in the same period, the phase of $^3D^1(\text{SO})_V$ arising from $V^1(\text{SO})$ is 7.0 hour as shown by the dashed line in fig. 11. The observed $^3D^1(\text{SO})$ can be regarded as a composition of $^3D^1(\text{SO})_V$ and that $(^3D^1(\text{SO})_{Ge})$ due to the Compton-Getting effect, as

$$(17) \qquad\qquad ^3D^1(\text{SO}) = {}^3D^1(\text{SO})_{Ge} + {}^3D^1(\text{SO})_V .$$

We can obtain these two vectors by drawing a straight line through a point of
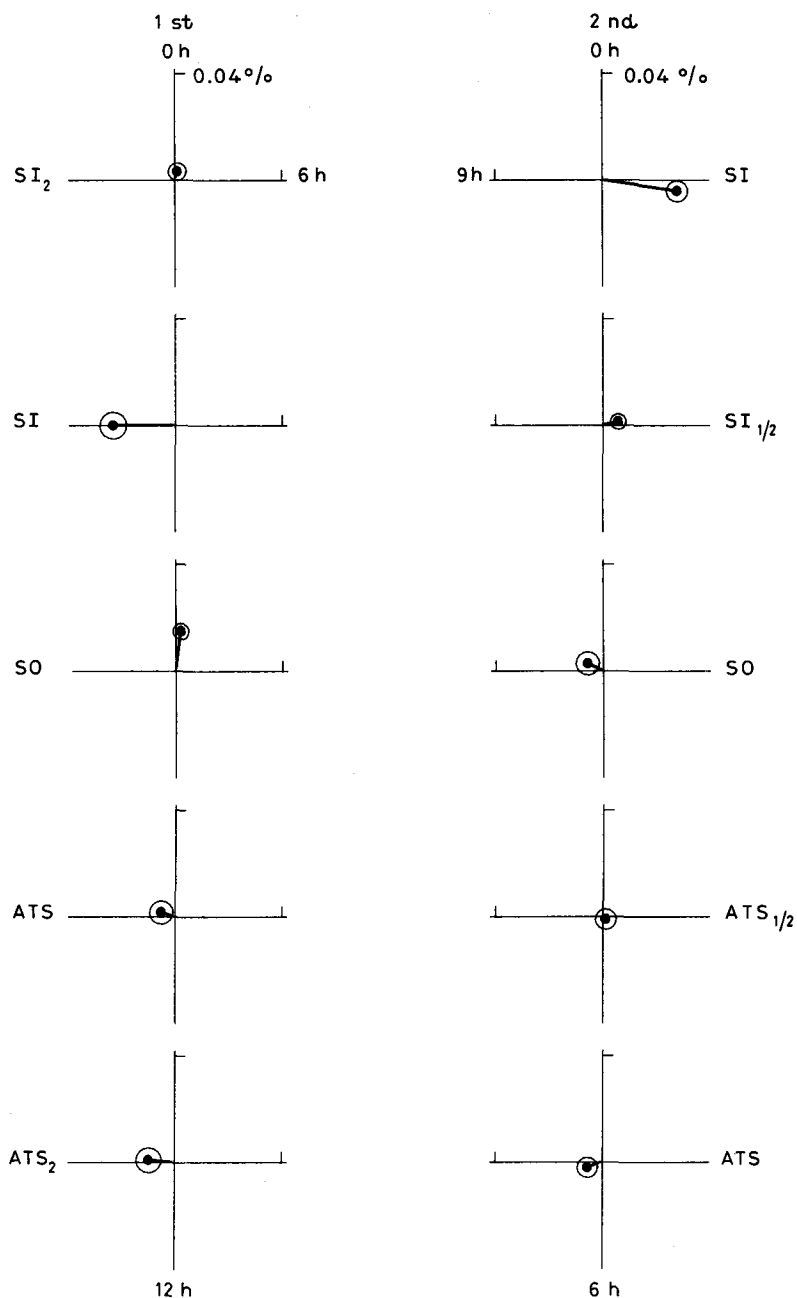
Fig. 9. – $^3\boldsymbol{D}^m(H)$. Solar, extended-sidereal and extended-antisidereal harmonic difference vectors ($^3\boldsymbol{D}^m = {}^3\boldsymbol{E}^m - {}^3\boldsymbol{W}^m$, $m = 1, 2$) in the periods 1975-78 and 1980-87. Errors shown by circles are estimated from the dispersion of yearly difference vectors.
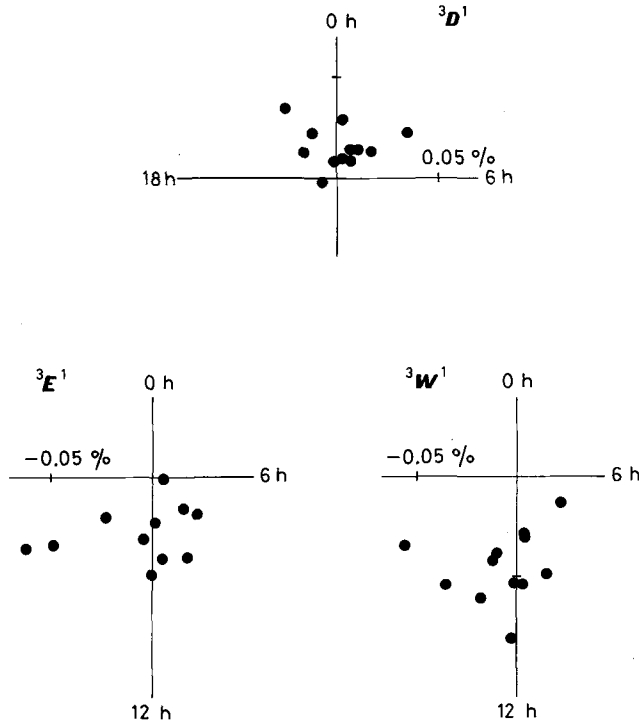
Fig. 10. – Yearly vectors of $^3E^1$(SO), $^3W^1$(SO) and $^3D^1$(SO) in the periods 1975-78 and 1980-87.

$^3D^1$(SO) parallel to the dashed line as shown in the figure. Inserting $^3D^1$(SO)$_{Ge}$ in eq. (15), we can estimate $\langle\psi\rangle$ at $\sim 12.2°$. It is noted here that even if we neglect the contribution of $^3D^1$(SO)$_V$ and regard $^3D^1$(SO) as $^3D^1$(SO)$_{Ge}$, the estimate of $\langle\psi\rangle$ is not much different from the value in the above. Using this value, we can estimate the contamination rate (r) of the spurious air showers mentioned above, as

(18)
$$r = \frac{|^3D^1(\text{SO})_V| \csc \langle\psi\rangle}{2|V^1(\text{SO})|} = 2.7\%,$$

in which $|V^1$(SO)$|$ is 0.19%. The rate is not much different from the value $(\sim 7\%)$ estimated previously. In order to confirm the reliability of the estimate of $\langle\psi\rangle$, we obtain $^3E^{*1}$(SO), $^3W^{*1}$(SO) and $^3C^1$(SO) according to the method shown in fig. 7 and compare $^3C^1$(SO) with a vector $^3U^1$(SO) which is obtained by subtracting G_e and rV^1(SO) from $^3F^1$(SO), as shown in fig. 12. These two vectors must coincide with each other, if the observed $^3F^1$(SO), $^3E^1$(SO) and $^3W^1$(SO) would be, respectively, the resultant of three vectors due to 1) the C-G effect, 2) the contamination of the single muon component and 3) the unidentified common
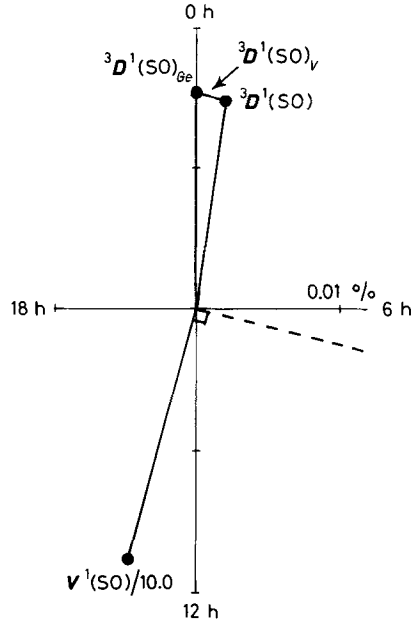
Fig. 11. – Decomposition of $^3D^1$(SO) into $^3D^1$(SO)$_{Ge}$ and $^3D^1$(SO)$_V$. $^3D^1$(SO): observed. $^3D^1$(SO)$_{Ge}$: Compton-Getting effect due to Earth's revolution around the Sun. $^3D^1$(SO)$_V$: contamination of low-energy muon component (cf. text). V^1(SO): vector of muon component observed by vertical telescope at Mt. Norikura. – – – direction of the difference vector $^3D^1$(SO)$_V$, derived from V^1(SO).
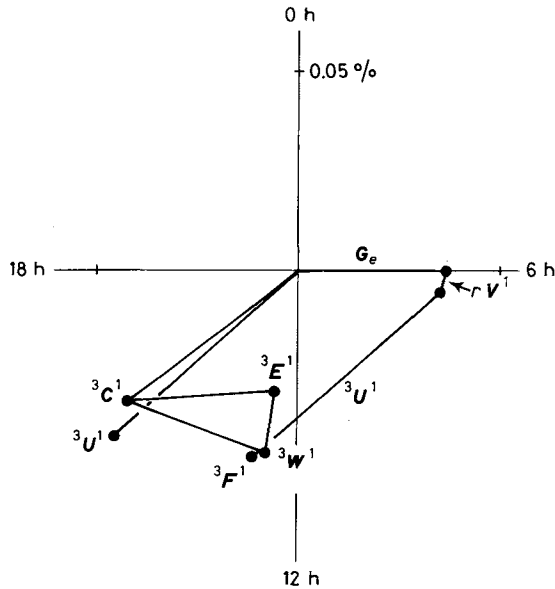
Fig. 12. – Comparison between common vector $^3C^1$(SO) and unidentified vector $^3U^1$(SO).

effect supposed to be the atmospheric effect. A fairly good coincidence supports the assumption and at the same time, it justifies the above estimate of $\langle \psi \rangle$. It is noted that the solar 1st harmonic vector contains considerably a large un-identified vector. The origin of this vector will be discussed later. We apply the same method as above to the statistically significant vectors $^3D^1$(SI) and $^3D^2$(SI) in fig. 9. These vectors are, respectively, decomposed into $^3C^m$, $^3E^{*m}$ and $^3W^{*m}$ as shown in fig. 13, and the space-originated vectors ($^3R^m$(SI)'s, $m = 1, 2$) for $^3E^{*m}$ and $^3W^{*m}$ are shown in fig. 14. $^3R^m$(SI)'s show some difference from the corresponding vectors $^3F^m$(SI)'s shown in the same figure. We call the difference ($^3U^m = {}^3F^m - {}^3R^m$, $m = 1, 2$) the unidentified vector. $^3U^m$'s ($m = 1, 2$) show fairly a good coincidence with the corresponding $^3C^m$'s ($m = 1, 2$), even though they are all within the statistical error. This seems to indicate that the omnidirectional air showers are influenced by some unidentified effect almost comparable with $^3C^m$(SI), ($m = 1, 2$) and that $^3R^m$(SI) ($m = 1, 2$) is due to the galactic anisotropy.

On the basis of these facts, it is concluded that:

1) The sidereal 1st and 2nd harmonic vectors $^iF^m$(SI)'s, ($m = 1, 2$) are statistically significant.

2) These vectors can be regarded as being mainly due to the galactic anisotropies, as they approximately coincide with the corresponding $^3R^m$(SI)'s derived from $^3D^m$(SI)'s. But they might contain some unidentified vectors $^3U^m$(SI)'s, ($m = 1, 2$) which can be regarded as corresponding common vectors $^3C^m$(SI)'s, ($m = 1, 2$) derived from the directional air shower observations.

3) As above, there is a mutual consistency between sidereal variations obtained by the omnidirectional and directional air shower observations.
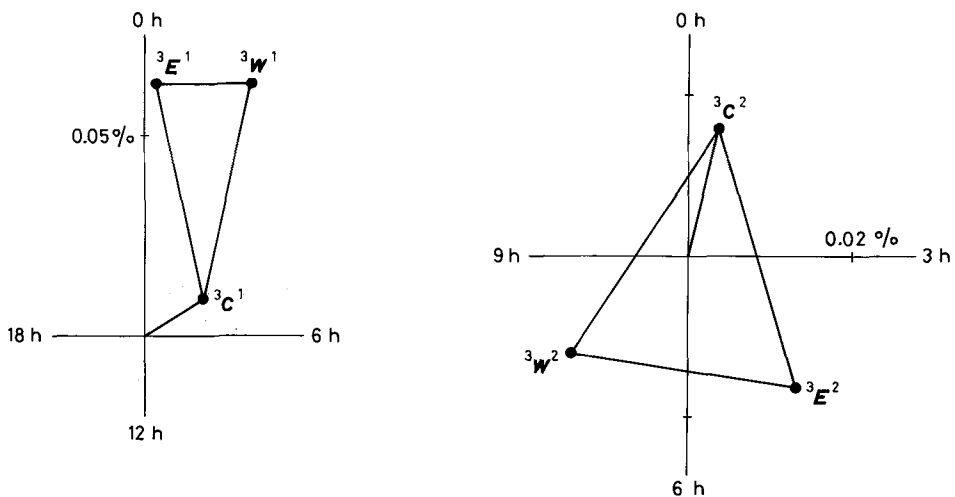
Fig. 13. – Decomposition of $^3E^m$(SI) and $^3W^m$(SI) into $^3E^{*m}$, $^3W^{*m}$ and $^3C^m$.
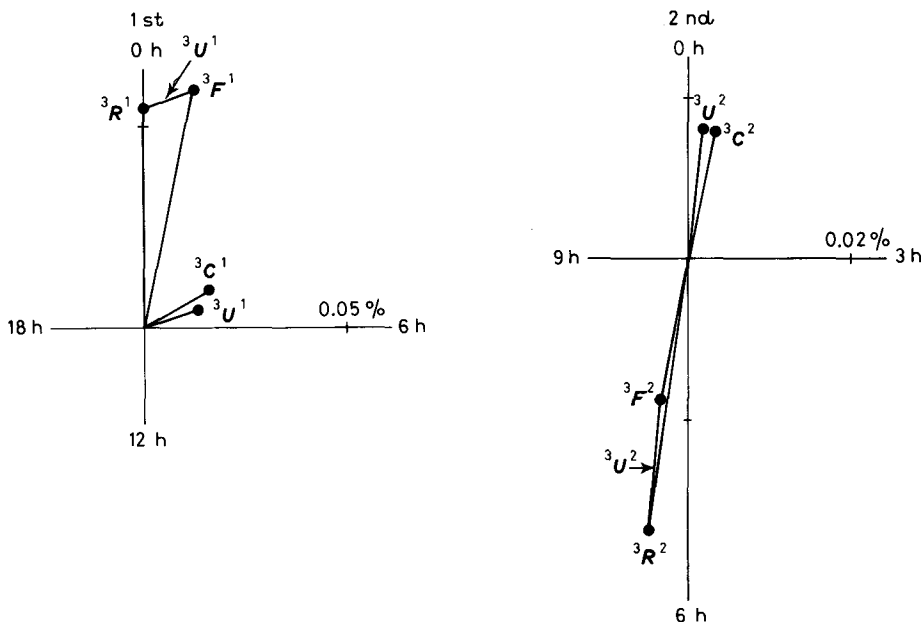
Fig. 14. – Comparison between $^3F^m$(SI) and $^3R^m$(SI) and between $^3U^m$(SI) and $^3C^m$(SI). $^3U^m$(SI) $= {}^3F^m$(SI) $- {}^3R^m$(SI).

4) These variations show fairly good agreement with those observed by other groups, as shown in fig. 15.

5) Solar diurnal variation is composed of three terms, one is due to the Compton-Getting effect produced by the Earth's revolution, the second is the
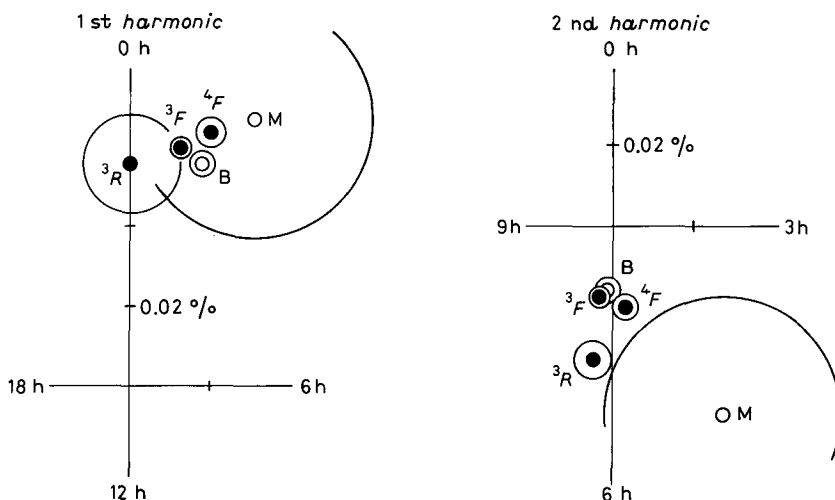
Fig. 15. – Comparison of the sidereal variations with those observed by other groups. B: Baxan [Alexeenko et al. ([7])]. M: Peak Musala [Gombosi et al. ([6])].

contamination of solar diurnal variation of muon component and the third is the common vector $^3C^1$(SO) probably due to the atmospheric effect. As can be seen in fig. 12, $^3C^1$(SO) is even greater than G_e due to the C-G effect. Its origin will be discussed later.

6) Although other harmonic vectors $^iF^m(H)$'s in table V are also statistically significant, their origin cannot be regarded as being due to some anisotropy in space, because the corresponding difference vectors $^3D^m(H)$'s cannot be regarded statistically well significant.

In the above, we have shown that the observed sidereal first and second harmonic vectors are due to the galactic anisotropy. In addition to these vectors, we point out also the existence of the sidereal third harmonic vector. As can be seen in table VIII, $^3F^3$(SI) is 4.7 times as large as its error. Mutual relation

TABLE VIII. – Sidereal 3rd harmonic vectors; $^3F^3$(SI), $^4F^3$(SI), $^3E^3$(SI), $^3W^3$(SI) and $^3D^3$(SI). Errors are estimated from the dispersion of yearly vectors. Figures in parentheses express the ratio of the amplitude to the error.

	Amplitude ($\cdot 10^{-4}$ %)	phase (h)		amplitude ($\cdot 10^{-4}$ %)	phase (h)
$^3F^3$(SI)	75 ± 16 (4.7)	7.2 ± 0.3	$^3E^3$(SI)	87 ± 39 (2.2)	6.0 ± 0.5
$^4F^3$(SI)	95 ± 28 (3.4)	7.9 ± 0.4	$^3W^3$(SI)	76 ± 24 (3.2)	7.9 ± 0.6
			$^3D^3$(SI)	110 ± 48 (2.3)	5.0 ± 0.5

among $^3F^3$(SI), $^3E^3$(SI), $^3W^3$(SI) and $^3R^3$(SI), derived from $^3D^3$(SI), are also shown in fig. 16. Fairly a good agreement between $^3F^3$(SI) and $^3R^3$(SI) indicates the existence of the third order $(n = 3)$ anisotropy of galactic origin. It is emphasized here that one of the phases of $^3F^3$(SI) (23.2 hour) nearly coincides with those phases of $^3F^1$(SI) and $^3R^1$(SI) in fig. 14 and further that they are approximately perpendicular to the phases (6.2, 18.2 hour) of $^3F^2$(SI) in real space (cf. fig. 14). These phase relations are schematically shown in fig. 17. As will be discussed in the following section, these phase relations can be produced by an axis-symmetric anisotropy in space, and the existence of the third harmonic vector provides some clue for the estimation of the three-dimensional spatial structure of the anisotropy.

Finally, we show in fig. 18 the hourly behaviour of the sidereal time variation of air showers $^3F(t_{SI})$ and $^4F(t_{SI})$ from which those harmonic vectors mentioned in the above have been derived. In the figure, the difference ($^3D(t_{SI})$, $t_{SI} = 1, 2, ..., 24$ hour) between directional air shower intensities $^3E(t_{SI})$ and $^3W(t_{SI})$ is also shown at the bottom. By taking the difference, one can eliminate the atmospheric effect as mentioned previously. Using $^3D(t_{SI})$, we can obtain the
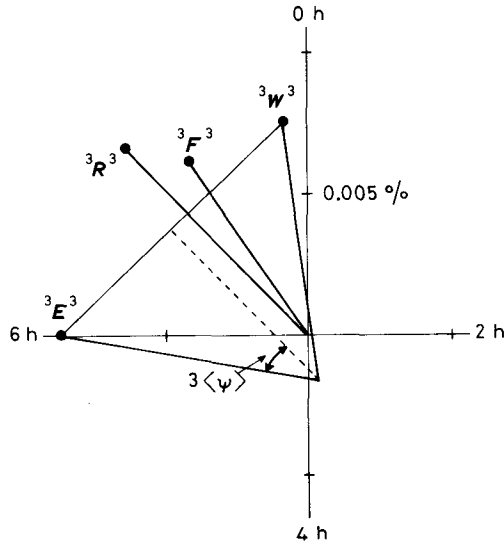
Fig. 16. – Average sidereal third harmonic vectors. ${}^3F^3$(SI) in 1973-1987. ${}^3E^3$(SI), ${}^3W^3$(SI) and ${}^3R^3$(SI) in 1975-1978 and 1980-1987.

differential $(\mathrm{d}/\mathrm{d}t)^3R(t_{\mathrm{SI}})$ of the space-originated intensity variation ${}^3R(t_{\mathrm{SI}})$, as

$$(19) \qquad \frac{\mathrm{d}}{\mathrm{d}t}{}^3R(t_{\mathrm{SI}}) = \frac{{}^3D(t_{\mathrm{SI}})}{2\langle\psi\rangle/15} \; (\%/\text{hour}),$$

where $\langle\psi\rangle$ is given by eq. (15). By integrating eq. (19), we can obtain ${}^3R(t_{\mathrm{SI}})$
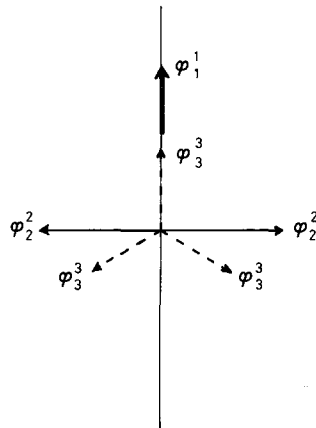
Fig. 17. – Schematic representation of the directions of maximum intensity due to the sidereal first to third harmonic vectors in the equatorial plane.
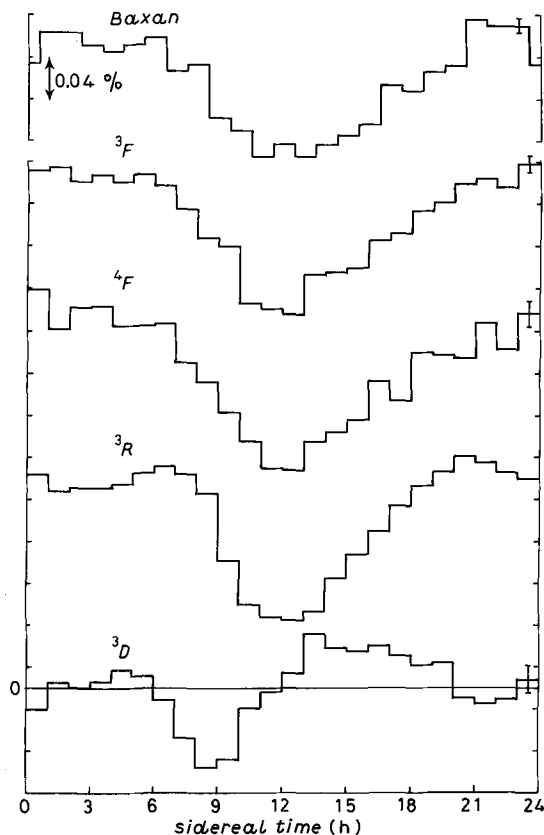
Fig. 18. – Hourly behaviour of sidereal daily variation of air showers. $^3D(t_{SI}) = {}^3E(t_{SI}) - {}^3W(t_{SI})$. $^3R(t_{SI})$: intensity variation free from the atmospheric effect, derived from $^3D(t_{SI})$ (cf. eq. (20)). Baxan: time variation of air showers at Baxan [Alexeenko and Navara[19]].

which is free from the atmospheric effect, as

(20)
$$\begin{cases} {}^3R(t_{SI}) = \int \left\{ \dfrac{d}{dt} {}^3R(t_{SI}) \right\} dt_{SI}, \\[4mm] {}^3R(t_{SI} + 1) = \displaystyle\sum_{t_{SI}=1}^{t_{SI}} \dfrac{{}^3D(t_{SI})}{2\langle\psi\rangle/15} \ (\%) \end{cases} \quad (t_{SI} = 1, 2, ..., 24\,\text{hour}).$$

The time variation of $^3R(t_{SI})$ is shown in the figure. The curve is very similar to those of ^3F and ^4F but slightly different from them. The deviation can be regarded as being due to the contamination of the atmospheric effects in $^3F(t_{SI})$ and $^4F(t_{SI})$ (cf. fig. 14). In the figure, the time variation observed at Baxan by

Alexeenko and Navara[19] is also shown, for comparison. One can see fairly a good coincidence among them. These variations, especially $^3R(t_{SI})$, are characterized by a plateau in a region of 19 hour-8 hour and a V-shaped sink with a bottom at ~ 12 hour. As such a time profile is rather artificial and is quite different from a sinusoidal curve, it seems difficult to be produced by a simple diffusion process of cosmic rays in the galactic space. The origin of the variation will be discussed in the last section.

As mentioned previously, we have observed also 36-fold air showers (^{36}F) in order to obtain the energy spectrum of the sidereal first and second harmonic vectors. The characteristic of ^{36}F are listed in table I. The sidereal harmonic vectors averaged for the period of 1978-1987 are listed in table IX. The errors

TABLE IX. – *Sidereal 1st and 2nd harmonic vectors* $^{36}F^m$(SI)'s *in the period* 1978-1987. *Errors are estimated from the dispersion of yearly vectors.*

	$^{36}F^1$(SI)	$^{36}F^2$(SI)
$A(\%)$	0.0250 ± 0.0148	-0.0118 ± 0.0242
$B(\%)$	-0.0044 ± 0.0183	0.0055 ± 0.0216

attached to these vectors are derived from the dispersion of yearly vectors. Contrary to our expectation, the amplitudes of these vectors are very small. The physical implication of these vectors will be discussed in the next section.

We now discuss the origin of $^3U^1$(SO) (or $^3C^1$(SO)) in fig. 12. As pointed out previously, we cannot attribute this vector to the atmospheric temperature effect, as the temperature coefficient (α) is extremely small (cf. table IV). The only possible origin of $^3C^1$(SO) might be the wind effect to the pressure observation. Although we have no wind data, we try to find out the trace of the wind effect by the following method. We assume that the strong wind blows at the time when the pressure variation is large or at the time when the temperature variation is large; most probably at the former time. On these assumptions, we divide data into two groups according to the magnitude of the amplitude of the solar first harmonic vectors of the pressure (or the temperature). If the assumption is correct, the solar first harmonic vectors of air showers of the two groups must show considerable difference from each other. On the left and right of fig. 19, we show the pressure-selected and temperature-selected $^3F^1$(SO) and $^3F^m$(SI). At a glance, the temperature-selected $^3F^1$(SO)'s are not much different from each other. On the other hand, the pressure-selected $^3F^1$(SO)'s show remarkable difference in their phase. These vectors $^3F^1$(SO)'s contain the terms G_e and rV^1(SO), (cf. fig. 12). If we eliminate these terms from

[19] V. V. ALEXEENKO and G. NAVARA: *Lett. Nuovo Cimento*, **42**, 321 (1985).
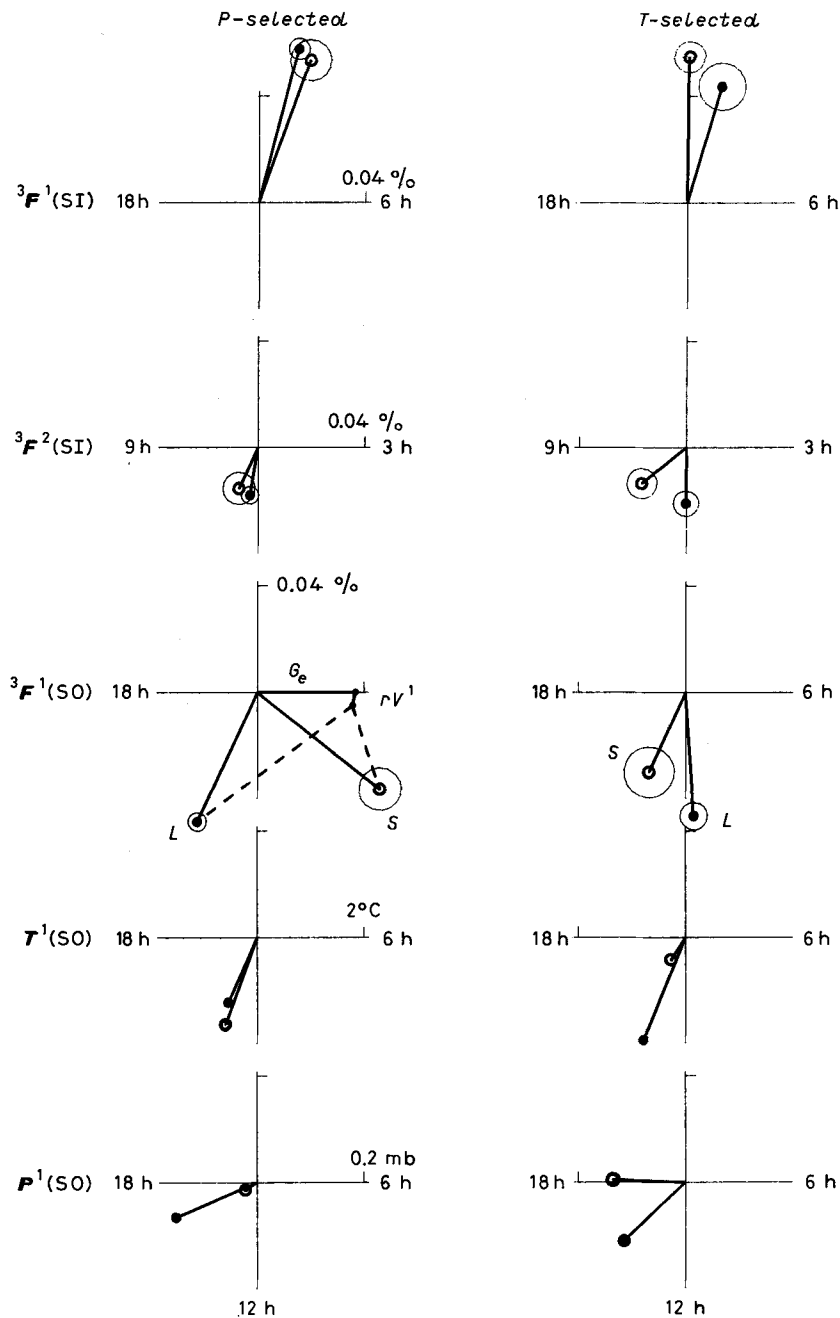
Fig. 19. – Pressure- and temperature-selected harmonic vectors $^3F^1$(SO) and $^3F^m$(SI). L/S expresses the average of vectors for days when the amplitude of the first harmonic vector (P^1 or T^1) of the pressure or temperature is greater/less than its average ($\langle P^1 \rangle$ or $\langle T^1 \rangle$).

$^3\boldsymbol{F}^1$(SO)'s, we get dashed vectors as shown in the figure. As the temperature effect is negligibly small and also as the dashed vectors cannot be regarded as a result of the improper pressure correction because of their nonparallelism with the pressure vector, the origin of the vectors would be the wind effect on the barometer observation. Note that a similar result can be derived from the directional air showers. As another indication for the existence of the wind effect to the barometer observation, we may point out the characteristic difference between the daily variations of the pressure at Mt. Norikura (2770 m above sea level) and at Nagoya (77 m above s.l.). As can be seen in fig. 1, the barometer at Nagoya shows the usual pattern; that is, the minimum value appears in the afternoon when the atmospheric temperature is about maximum. On the contrary, the pressure change at Mt. Norikura is somewhat extraordinary, that is, the minimum value appears early in the morning when the temperature is minimum. The transition of the occurrence time of the minimum pressure from the afternoon to the early morning could be regarded as being due to the negative wind effect to the pressure. If the strong wind blows in the early morning, the pressure lowers down and the inversion of the minimum could be expected. In fact, the observed wind velocity seems to support this assumption as can be seen in fig. 1, although its observation period is short and also its amplitude is not large enough to explain the inversion of the minimum quantitatively. It is emphasized here that the air shower station is located at the saddle point on Mt. Norikura in the central region of Japan Alps and the wind across the Alps is always upwards regardless of its direction, thus producing the negative pressure effect. If we could observe the wind velocity not disturbed by the friction against the ground, the amplitude of its daily variation would be enhanced. If the amplitude of the velocity is 1m/s in case of the regression eq. (9) or 3.5m/s in case of eq. (4), the pressure change is about $(0.08 \div 0.09)$ mb which is enough to produce $^3C^1$(SO) (or $^3U^1$(SO)) in question. Such an interpretation could be supported by the following fact. If we make the hourly solar time variation $^3R(t_{SO})$ from $^3D(t_{SO})$ according to the procedure defined by eqs. (19) and (20) and subtract it from $^3F(t_{SO})$, the difference $\Delta^3F(t_{SO})(= {}^3F(t_{SO}) - {}^3R(t_{SO}))$ is of the
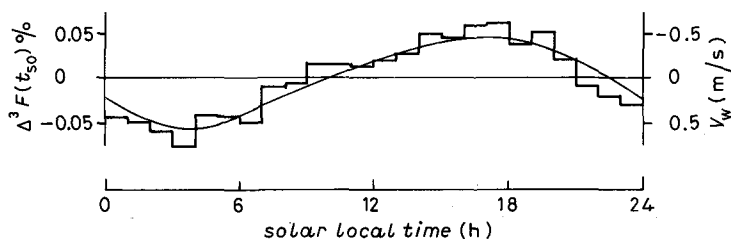
Fig. 20. – $\Delta^3F(t_{SO})$; solar time variation not due to anisotropy. $\Delta^3F(t_{SO}) = {}^3F(t_{SO}) - {}^3R(t_{SO})$. The definition of $^3R(t_{SO})$ should be referred to the text. Thin curve is the solar time variation of the atmospheric wind velocity $V_W(t_{SO})$ in 1972. The similarity between the two variations suggests the wind-origin hypothesis of $\Delta^3F(t_{SO})$.

atmospheric origin. As the pressure correction has already been made and also as the temperature effect is negligibly small, $\Delta^3 F(t_{SO})$ could be regarded as being due to the wind effect. Figure 20 compares $\Delta^3 F(t_{SO})$ with $-V_W(t_{SO})$ reproduced from fig. 1. Fairly a good coincidence between these curves supports the above interpretation. It is emphasized however that the wind does not give much influence on $^3F^2(SO)$ and $^3F^m(SI)$'s ($m = 1, 2$), as can be seen in fig. 19 and therefore that it does not affect the previous conclusion as to the average sidereal variation.

4'3. *Dependence on the polarity of the polar magnetic field of the Sun.* – According to the simulation of the heliomagnetospheric modulation of galactic anisotropy by Nagashima *et al.* [20] and Nagashima and Morishita [21], the sidereal harmonic vectors and their annual and semi-annual variations produced from the anisotropy show the polarity dependence of the polar magnetic field of the Sun. The modulation would be observed mainly in the rigidity region $< 10^{13}$ V and it especially dominates in the region of $p \sim 10^{12}$ V. As cosmic rays with $p \sim 10^{12}$ V can produce air showers detectable with the present shower array, the observed sidereal variation and its annual modulation might be subject to the polarity dependence mentioned above. Fortunately, the polarity reversal occurred almost in the middle of the observation period; the solar South Pole appears to have made the transition from toward to away between May and December of 1979, while the North Pole reversed its polarity between January and May 1980 (cf. solar magnetic field synoptic charts published monthly in Solar-Geophysical Data, U.S. Dept. of Commerce, Boulder, Colo. and also Hoeksema and Scherrer [22]). We can test the above hypothesis by dividing data into two groups, one is in the period (1973-1978) of the positive polarity state when the magnetic field is away from the Sun at the North Pole and toward the Sun at the South Pole and the other is in the period (1981-1987) of the negative polarity state when the fields at both poles are reversed. We define the difference vectors between $^3F^m$'s ($^3D^m$'s) in the positive (P) and negative (N) states as

$$(21) \quad \begin{cases} {}^3F^m(P - N) = \{{}^3F^m(P) - {}^3F^m(N)\}/2, \\ {}^3D^m(P - N) = \{{}^3D^m(P) - {}^3D^m(N)\}/2, \end{cases} \quad m = 1, 2.$$

These vectors are shown respectively in fig. 21. One can see some statistically

[20] K. NAGASHIMA, I. MORISHITA and S. YASUE: *Planet. Space Sci.*, **30**, 879 (1982); K. NAGASHIMA, I. MORISHITA and S. YASUE: *Planet. Space Sci.*, **31**, 1259 (1983).

[21] K. NAGASHIMA and I. MORISHITA: *Report of Cosmic Ray Res. Lab., Nagoya Univ.*, no. 8 (1983).

[22] J. T. HOEKSEMA and P. H. SCHERRER: *World Data Center A for Solar-Terrestrial Phys. Rep.*, UAG-94 (1986).
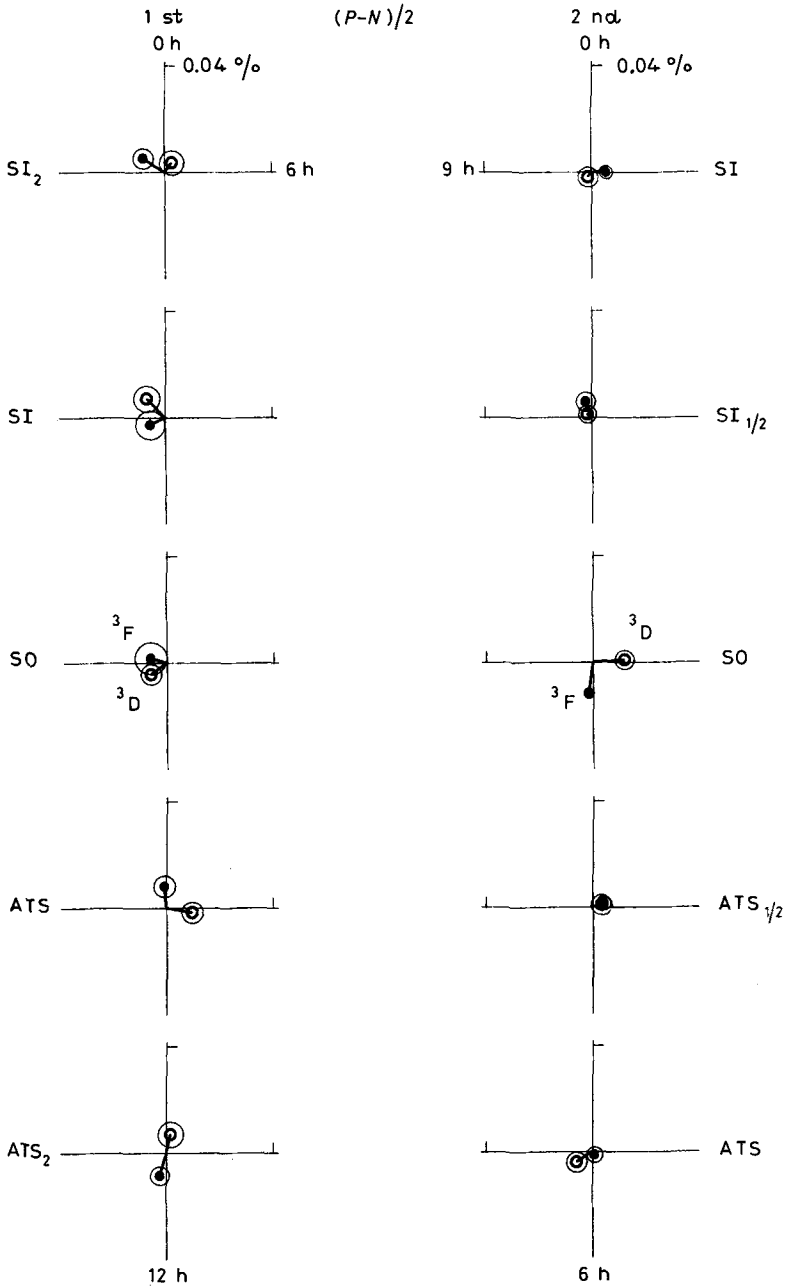
Fig. 21. – $^3F^m(H, P - N)$ and $^3D^m(H, P - N)$. Dependence of harmonic vectors on the polarity reversal of the polar magnetic field of the Sun. The definition of these vectors is shown in eq. (21). P: positive polarity state (1978), N: negative polarity state (1981-1987). ● $^3F^m$, ○ $^3D^m$.

significant vectors. Among them, $^3\boldsymbol{F}^2(\text{SO}, P - N)$ is six times and $^3\boldsymbol{D}^2(\text{SO}, P - N)$ is three times greater than the corresponding dispersions and statistically significant. Furthermore, these two vectors are almost perpendicular to each other as expected from the phase relation produced by some anisotropy in space (cf. fig. 21). It is emphasized here that these vectors are produced as a result of the phase reversal of $^3\boldsymbol{F}^2$ and $^3\boldsymbol{D}^2$ occurred during or near the transition period of the polarity reversal (1979-1980), as can be seen in the sum harmonic dial of their yearly vectors in fig. 22. In association with these phase reversals, the sidereal
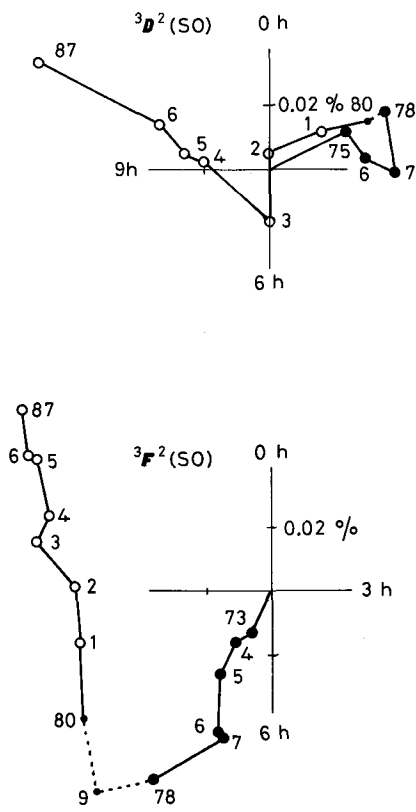
Fig. 22. – Sum harmonic dials of $^3\boldsymbol{F}^2(\text{SO})$ and $^3\boldsymbol{D}^2(\text{SO})$. Figures attached to the vector express year. Vectors in the positive polarity state (1978) are expressed by solid circles and those in the negative state (1981-1987) by open circles. Vectors in the transition period are shown by dotted lines.

first and second harmonic vectors $(^3\boldsymbol{F}^m(\text{SI})\text{'s}, m = 1, 2)$ also change their phase as shown in fig. 23. Although the phase change of $^3\boldsymbol{F}^1(\text{SI})$ is not so much clear, that of $^3\boldsymbol{F}^2(\text{SI})$ can be regarded as statistically significant. The cause of these phase reversals and phase changes will be discussed in relation to the polarity reversal of the heliomagnetosphere. It is noted finally that the existence of the
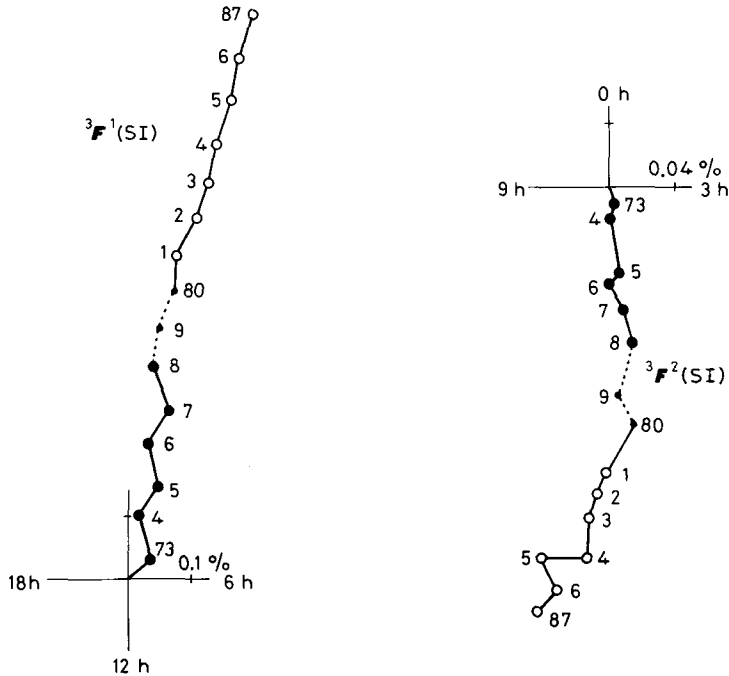
Fig. 23. – Sum harmonic dials of $^3F^1$(SI) and $^3F^2$(SI) in the period 1973-1987. Caption is the same as in fig. 22.

polarity dependence does not much affect the previous conclusion as to the average sidereal variation, because the period of the observation contains almost the same partition of P-and N-state and therefore the effect of the dependence becomes negligibly small by taking the average of the vectors for all the period.

5. – Discussion and conclusion.

It is concluded that:

1) We have confirmed the existence of the sidereal diurnal, semidiurnal and tridiurnal variations of air showers with median energy $\sim 10^{13}$ eV.

2) The observation of the directional air showers has proved that these variations in the above are mostly due to some anisotropy or anisotropies and not due to the atmospheric origin.

3) The directional air shower observation has proved further that the anisotropy (or anisotropies) is of galactic origin, because there are no other variations of nonatmospheric origin, comparable with these variations in magnitude, except for that due to C-G effect of solar origin. Especially, the lack

of the large solar diurnal and semidiurnal variations of solar origin denies the possibility of producing these sidereal variations by their annual modulation.

4) The sidereal diurnal and semidiurnal harmonic vectors $^3F^m$(SI), $^4F^m$(SI) and $^3R^m$(SI) show considerably a good coincidence with the corresponding vectors of air showers observed at Peak Musala and at Baxan (cf. fig. 15). Furthermore, it is noteworthy that the hour-to-hour variations of ^3F and ^3R show quite a good agreement with that observed at Baxan (cf. fig. 18). These variations, especially that of $^3R(t_{SI})$, have a time profile characterized by a plateau in a region of 19 hour-8 hour and a V-shaped sink with a bottom at ~ 12 hour.

5) Some harmonic vectors ($^3F^m$, $^3D^m$) changed their phase at the epoch (1979-1980) when the polar magnetic field of the Sun reversed its polarity (cf. fig. 21-23).

The main part of the above conclusion is based largely on the observation of directional air showers and also on the confirmation of the existence of the solar diurnal variation due to the Compton-Getting effect arising from the Earth's revolution around the Sun. It is emphasized here that the existence of sidereal variations of galactic origin could be proved even without the confirmation of C-G effect, as far as the mutual seperation between $^3E^m$(SI) and $^3W^m$(SI) is statistically significant as can be seen in figs. 8 and 9. However, without using the above effect, one cannot derive the magnitude of the original vector $^3R^m$ from $^3D^m$($m = 1, 2$) (cf. fig. 7).

In the following, we discuss the nature of the galactic anisotropy responsible for these sidereal variations. We first study the structure of the anisotropy in space inferred from the sidereal harmonic vectors averaged for the whole period. The most simple anisotropy is produced by the well-known Compton-Getting effect arising from the motion of the solar system relative to some reference coordinate system where cosmic rays are supposed to be isotropic. The proper motion of the solar system relative to the nearby stars has been regarded as the most promising candidate for the origin of the C-G effect, and the motion of the solar system relative to the surrounding interstellar gas also could be one of the candidates[23]. Unfortunately, however, we cannot determine its direction (α: right ascension, δ: declination) from the observation of sidereal time variation of cosmic rays unless the cosmic-ray absolute intensity can be observed, and we have to be satisfied by knowing α only, even if the variation is due to only this effect[24]. As the observed first harmonic vector has a phase quite different from that expected from such a kind of effect, we have to consider another kind of

[23] E.g., W. McCLINTOCK, R. C. HENRY, J. L. LINSKY and H. W. MOOS: Astrophys. J., 225, 465 (1978); J. M. AJELLO: Astrophys. J., 222, 1068 (1978).
[24] K. NAGASHIMA: Rep. Ionos. Space Res. Japan, 25, 189 (1971).

anisotropy in space, which could produce also the observed higher-order harmonic vectors. We assume that as the first approximation, the anisotropy can be expressed simply by an axis-symmetric function $F(\chi)$ defined by only the pitch angle (χ) with respect to some reference axis specified by the right ascension (α_R) and declination (δ_R). The function can be expanded in a series of spherical functions in the Earth's equatorial coordinate system [24], as

$$(22) \qquad F(\chi) = \sum_{n=0}^{\infty} \eta_n P_n^0(\cos \chi),$$

$$(23) \qquad \eta_n P_n^0(\cos \chi) = \sum_{m=0}^{n} \eta_n P_n^m(\cos \theta_R) P_n^m(\cos \theta) \cos \frac{2m\pi}{24}(\alpha - \alpha_R),$$

where θ is the co-declination defined by

$$\theta = \pi/2 - \delta.$$

In the equations, θ and α express the incident direction of the cosmic rays and P_n^m is the semi-normalized associate spherical function [25], as

$$(24) \qquad \begin{cases} P_n^m(x) = P_{n,m}(x) & \text{for } m = 0, \\[2mm] P_n^m(x) = \sqrt{2 \dfrac{(n-m)!}{(n+m)!}}\, P_{n,m}(x) & \text{for } m \neq 0, \end{cases}$$

in which $P_{n,m}(x)$ is the ordinary «associate spherical function». In the following discussion, each term on the right-hand side of eq. (23) is treated, for simplicity, as the m-th harmonic vector $\boldsymbol{a}_n^m$ with its components A_n^m and B_n^m as

$$(25) \qquad \begin{cases} A_n^m = \eta_n P_n^m(\cos \theta_R) P_n^m(\cos \theta) \cos \dfrac{2m\pi}{24} \alpha_R, \\[3mm] B_n^m = \eta_n P_n^m(\cos \theta_R) P_n^m(\cos \theta) \sin \dfrac{2m\pi}{24} \alpha_R. \end{cases}$$

For the explanation of the observed second harmonic vector, we need at least up to the second-order anisotropy $(n = 2)$. The anisotropy for $n = 2$ produces also $\boldsymbol{a}_2^1$ which is quite different in character from the one $(\boldsymbol{a}_1^1)$ produced from the first-order anisotropy $(n = 1)$. Table X shows the characteristic dependence of the phase φ_n^m of $\boldsymbol{a}_n^m$ on η_n, $\delta_R(= \pi/2 - \theta_R)$ and $\delta(= \pi/2 - \theta)$. One can infer the structure

[25] S. CHAPMAN and J. BARTELS: *Geomagnetism*, Vol. 2 (Oxford University Press, Oxford, 1940), p. 611.

TABLE X. – *Characteristics of the phase* φ_n^m *of the vector* $\boldsymbol{a}_n^m$ *in* eq. (25), *produced from the axis-symmetric function* $F(\chi)$. *Phase is expressed in units of hour.* α_R *is in units of degree.*

φ_n^m	η_n	δ_R	North 26.6°	δ 0°	South −26.6°
φ_1^1	$+$			$\alpha_R/15$	
φ_2^1	$+$	$+$	$\alpha_R/15$		$(\alpha_R+\pi)/15$
		$-$	$(\alpha_R+\pi)/15$		$\alpha_R/15$
	$-$	$+$	$(\alpha_R+\pi)/15$		$\alpha_R/15$
		$-$	$\alpha_R/15$		$(\alpha_R+\pi)/15$
φ_3^1	$+$	$|\delta_R|>26.6$	$\alpha_R/15$	$(\alpha_R+\pi)/15$	$\alpha_R/15$
		$|\delta_R|<26.6$	$(\alpha_R+\pi)/15$	$\alpha_R/15$	$(\alpha_R+\pi)/15$
	$-$	$|\delta_R|>26.6$	$(\alpha_R+\pi)/15$	$\alpha_R/15$	$(\alpha_R+\pi)/15$
		$|\delta_R|<26.6$	$\alpha_R/15$	$(\alpha_R+\pi)/15$	$\alpha_R/15$
φ_2^2	$+$			$\alpha_R/30$	
	$-$			$(\alpha_R+\pi)/30$	
φ_3^2	$+$	$+$	$\alpha_R/30$		$(\alpha_R+\pi)/30$
		$-$	$(\alpha_R+\pi)/30$		$\alpha_R/30$
	$-$	$+$	$(\alpha_R+\pi)/30$		$\alpha_R/30$
		$-$	$\alpha_R/30$		$(\alpha_R+\pi)/30$
φ_3^3	$+$			$\alpha_R/45$	
	$-$			$(\alpha_R+\pi)/45$	

of the anisotropy from these phase relations. The anisotropy specified by $n=2$ and $\eta_2>0$ is the well-known two-way anisotropy presented by Jacklyn [26], which is characterized by the equal phase (in units of hour) of the first and second harmonic vectors. In the present observation, the possibility of the anisotropy of

[26] R. M. JACKLYN: *Nature*, **211**, 690 (1966); R. M. JACKLYN: *Proc. Astron. Soc. Aust.*, **6**, 425 (1986).

this sort is excluded because the observed phase difference in question is quite different from zero as can be seen in fig. 24 and also because this phase difference could not become zero even if some correction due to C-G effect were applied to the first harmonic vector. The phase difference between $^3F^1$(SI) and $^3F^2$(SI) or between $^3R^1$(SI) and $^3R^2$(SI) is 5.5 hours or 6.3 hours and approximately coincides with 6 hours expected from the axis-symmetric anisotropy with $\eta_2 < 0$. The phase relation between these vectors becomes worse if we eliminate from $^3F^1$(SI) or $^3R^1$(SI) the vector G_p due to the C-G effect caused by the proper motion of solar system ($\alpha_R = 17.9$ h, $\delta_R = 20°$, $v = 20$ km/s). The corrected vector is shown by the dashed line on the left-hand harmonic dial in fig. 24, and the
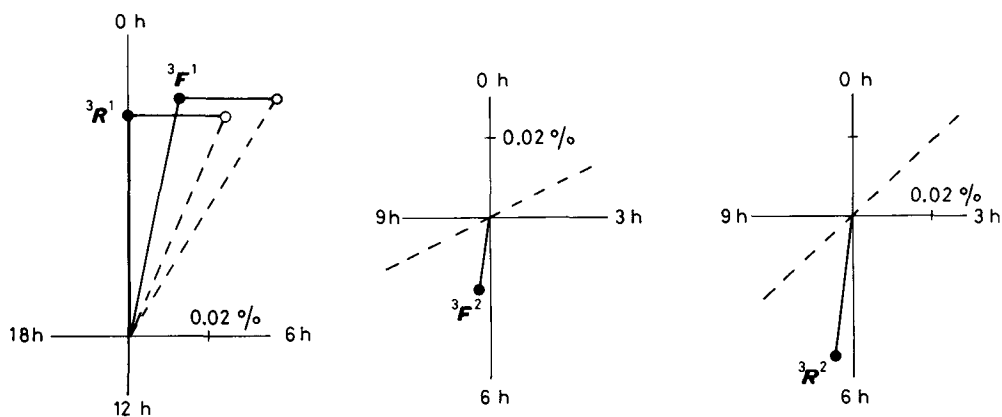
Fig. 24. – Influence of Compton-Getting effect of galactic origin. ● observed vectors; ○ vectors corrected for the Compton-Getting effect due to the proper motion of the Solar system. Dashed lines on the 2nd harmonic dials express, respectively, the phase expected from the axis-symmetric anisotropies producing the corresponding first harmonic vectors corrected for Compton-Getting effect.

expected phase of the second harmonic vector produced from the axis-symmetric anisotropy responsible for the corrected vector is shown by the dashed line on the middle or right-hand harmonic dial. The observed phase of $^3F^2$(SI) or $^3R^2$(SI) is considerably different from the expected one. Even if we use the C-G effect (G_g) due to the motion of the solar system relative to the interstellar neutral gas ($\alpha_R = 252° \sim 288°$, $\delta_R = -15° \sim -17°$, $v \sim 22$ km/s) in substitution to G_p, we get a similar result to the above. This implies that we cannot get any positive support for the assumption that the galactic anisotropy consists of two axis-symmetric distribution with different reference axes, one is due to the C-G effect and the other is of another origin. It is noted however that even if we introduce G_g or G_p, the symmetry of the observed result is not much disturbed. We maintain the assumption of the symmetry of the space distribution in the following analysis. The right ascension (α_R) of the direction of the anisotropy would be about $0 \sim 1$ h, inferred from the phases mentioned above. Assuming that $\alpha_R = 0$, the observed

first and second harmonic vectors $(\boldsymbol{a}^1, \boldsymbol{a}^2)$ are given by

$$(26) \qquad \boldsymbol{a}^1(\theta) = \boldsymbol{a}^1_1(\theta_R, \theta) + \boldsymbol{a}^1_2(\theta_R, \theta), \quad \boldsymbol{a}^2(\theta) = \boldsymbol{a}^2_2(\theta_R, \theta).$$

If we can extract $\boldsymbol{a}^1_2(\theta_R, \theta)$ from $\boldsymbol{a}^1(\theta)$, we can determine θ_R by the following equation (cf. eq. (25)):

$$(27) \qquad \frac{|\boldsymbol{a}^1_2|}{|\boldsymbol{a}^2_2|} = \frac{|P^1_2(\cos\theta_R)\, P^1_2(\cos\theta)|}{P^2_2(\cos\theta_R)\, P^2_2(\cos\theta)} = 4\,|\mathrm{ctg}\,\theta_R\,\mathrm{ctg}\,\theta|.$$

The extraction can be made, using the observed vectors $\boldsymbol{a}^1(\theta_1)$ and $\boldsymbol{a}^1(\theta_2)$ at two stations:

$$(28) \qquad \boldsymbol{a}^1(\theta_1) = \boldsymbol{a}^1_1(\theta_R, \theta_1) + \boldsymbol{a}^1_2(\theta_R, \theta_1), \quad \boldsymbol{a}^1(\theta_2) = \boldsymbol{a}^1_1(\theta_R, \theta_2) + \boldsymbol{a}^1_2(\theta_R, \theta_2).$$

The best way to obtain $\boldsymbol{a}^1_2$ is to use data at two conjugate stations in the northern $(\theta_1 < \pi/2)$ and southern $(\theta_2 = \pi - \theta_1)$ hemispheres. In this case, $\boldsymbol{a}^1_2(\theta_R, \theta_1)$ is given by the following equation, as $\boldsymbol{a}^1_2$ is of North-South asymmetry (*i.e.* $\boldsymbol{a}^1_2(\theta_R, \theta_1) = -\boldsymbol{a}^1_2(\theta_R, \pi - \theta_1)$):

$$(29) \qquad \boldsymbol{a}^1_2(\theta_R, \theta_1) = \{\boldsymbol{a}^1(\theta_1) - \boldsymbol{a}^1(\theta_2)\}/2.$$

In the previous paper [1], we chose Poatina $(\delta = -42°)$ as the conjugate station for Mt. Norikura and used the result of the underground muon observation at the station $(E_m = 10^{12}\,\mathrm{eV}, \ x = 365\,\mathrm{m.w.e.})$ [27]. In the present paper, however, we do not use the data because of too much difference in their median energy. Generally, δ_R can be determined by using results observed at any two stations. The harmonic vectors $(m = 1, 2)$ at Baxan $(\delta_B \sim 43.4°)$ can be used in principle for this purpose. But, as the station is very close to Mt. Norikura in latitude, we cannot get a statistically significant result. As another method for the determination, we can use the first to third harmonic vectors at one station, if $F(\chi)$ can be assumed as

$$(30) \qquad F(\chi) = \begin{cases} F_0 & \text{for } \chi_0 \geqslant \chi \geqslant 0, \\ 0 & \text{for } \pi \geqslant \chi > \chi_0. \end{cases}$$

Such an assumption holds approximately as the time profile of the sidereal daily variation is characterized by a flat plateau and a V-shaped sink as shown in fig. 18.

[27] A. G. FENTON and K. B. FENTON: *Proceedings of the XIV International Cosmic Ray Conference, München, 1975*, 4, 1482.

In this case, the coefficients $(\eta_1, \eta_2, \eta_3, ...)$ of $F(\chi)$ in eq. (22) are given by

(31)
$$\begin{cases} \eta_1 = (3/4) F_0 \sin^2 \chi_0 , \\[2mm] \eta_2 = (5/4) F_0 \sin^2 \chi_0 \cos \chi_0 , \\[2mm] \eta_3 = (7/6) F_0 \sin^2 \chi_0 (5 \cos^2 \chi_0 - 1) , \\[2mm] \eta_4 = ... \end{cases}$$

These parameters are shown in fig. 25 as a function of χ_0. We can determine the unknown parameters $(F_0, \chi_0$ and $\delta_R)$ by the following equations:

(32)
$$\begin{cases} \boldsymbol{a}^1(\theta) = \boldsymbol{a}_1^1(\eta_1, \theta_R, \theta) + \boldsymbol{a}_2^1(\eta_2, \theta_R, \theta) + \boldsymbol{a}_3^1(\eta_3, \theta_R, \theta) , \\[2mm] \boldsymbol{a}^2(\theta) = \boldsymbol{a}_2^2(\eta_2, \theta_R, \theta) + \boldsymbol{a}_3^2(\eta_3, \theta_R, \theta) , \\[2mm] \boldsymbol{a}^3(\theta) = \boldsymbol{a}_3^3(\eta_3, \theta_R, \theta) . \end{cases}$$
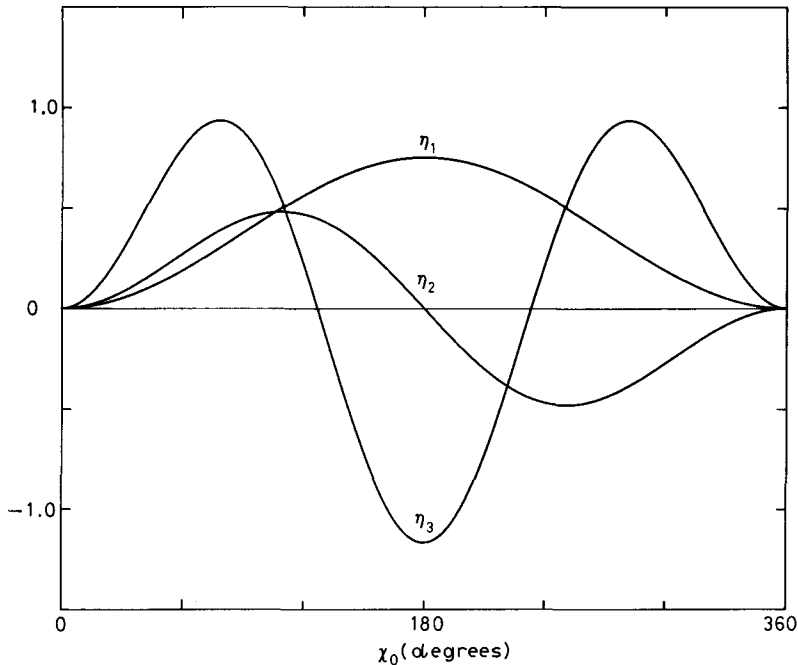
Fig. 25. – Spherical surface harmonic coefficients $(\eta_1, \eta_2, \eta_3, ...)$ of $F(\chi)$ in eq. (30) as a function of χ_0.

As mentioned previously, the sidereal first to third harmonic vectors observed at Mt. Norikura approximately satisfy the assumption of the axis-symmetry (cf. fig. 17) and therefore they can be used for the present analysis. However, as far

as we use $^3\boldsymbol{F}^m$(SI)'s ($m = 1, 2, 3$), we cannot find the solution of eq. (32). But, if we use the space-originated vectors ($|^3\boldsymbol{R}^1$(SI)$| = 0.0548\%$, $|^3\boldsymbol{R}^2$(SI)$| = 0.0341\%$, $|^3\boldsymbol{R}^3$(SI)$| = 0.0092\%$) derived from $^3\boldsymbol{D}^m$(SI)'s in tables VII and VIII, we get two alternative solutions, as shown in table XI. The direction of the anisotropy is

TABLE XI. – *Two sets of parameters of $F(\chi)$ in eq. (30), which satisfy eq. (32).*

Type	$F_0(\%)$	$\chi_0(°)$	$\alpha_R(°)$	$\delta_R(°)$	$l(°)$	$b(°)$	$\eta_1(\%)$	$\eta_2(\%)$	$\eta_3(\%)$
I	0.212	119	0	15	106	− 46	0.121	− 0.098	0.031
II	0.094	123	0	− 20	64	− 77	0.049	− 0.045	0.034

($\alpha_R = 0$ hour, $\delta_R = 15°$) or ($\alpha_R = 0$ hour, $\delta_R = -20°$). It is noted, however, that even in a region between these two directions ($\alpha_R = 0$, $\delta_R = 15° \sim -20°$), we can find the space distribution which approximately satisfies eq. (32). Therefore, the two values of δ_R in the above could be regarded as the boundary limit of the allowable direction of the anisotropy. For reference, we show one of the distribution of type II in table XI on the equatorial coordinates (α, δ) on the upper part in fig. 26 and also on the Galactic coordinates (l, b) on the lower part in fig. 26. The region covered by a group of concentric circles expresses the loss cone, in which direction less cosmic-ray intensity is observed. The centre direction of loss cone is marked by L.C. and its half angle is defined by $\pi - \chi_0$. The flow seems difficult to be attributed to the simple diffusion process as the time profile of $^3R(t_{SI})$ in fig. 18 is quite different in form from a sinusoidal curve, as pointed out previously. The following is a tentative model which might explain $^3R(t_{SI})$. The solar system is located near the boundary of the inner region where cosmic rays are isotropic and have higher density than those in the outer region. These two regions are connected by ordered magnetic lines of force along the direction of the anisotropy, characterized by gradually increasing magnetic field strength towards the outer region. Cosmic-ray particles are subject to orbital motion in the magnetic field without making many scatterings with the magnetic irregularities ($\Delta\boldsymbol{B}$) superposed on the ordered magnetic field ($\boldsymbol{B}$), and some of them fly away toward the outer region by the orbital motion. The loss cone is formed as a result of the mirror action by the afore-mentioned magnetic field configuration; that is, among the outgoing particles ($\pi/2 > \chi \geqslant 0$) near the solar system, those with $\chi > \pi - \chi_0$ return back into a region of $\chi_0 > \chi > \pi/2$ by the reflection near the boundary, while those with $\pi - \chi_0 > \chi > 0$ go into the outer region without reflection and instead, other low-density particles come into the inner region to fill the loss cone region ($\pi \geqslant \chi > \chi_0$). It is emphasized here that the direction of $\boldsymbol{B}$ is quite different from that of the motion of the neutral gas in the vicinity of solar system [23]. According to the present analysis, the direction of the anisotropy is bounded in the comparatively narrow region mentioned above, but even in the limited range, the change of the direction produces a
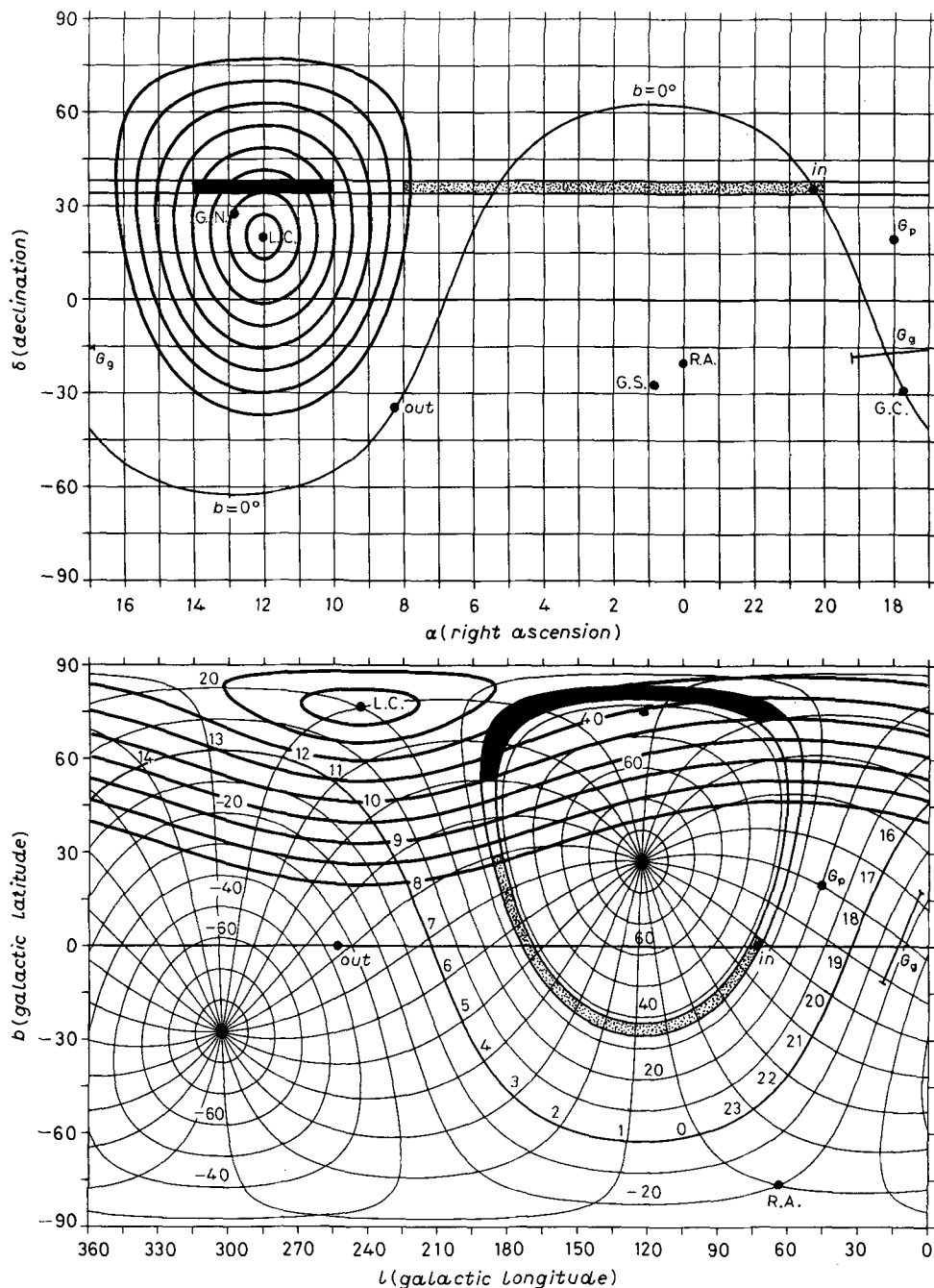
Fig. 26. – Space distribution of galactic anisotropy. Upper: on the equatorial coordinate (α, δ). Lower: on the galactic coordinate (l, b). Distribution is of the type II in table XI. The direction of the reference axis of the anisotropy is shown by R.A. The region covered by a group of thick circles with their centre at L.C. expresses the loss cone. Thin curves on the lower part express equatorial coordinates. The scanning direction of the air shower telescope is expressed by straight or curved belt; its dotted part indicates the plateau region of $^3R(t_{SI})$ in fig. 18 while the black part the bottom of the V-shaped sink. The symbol ' in and out ': Spiral-in and out of the Orion arm. G.C., G.N., and G.S: Galactic center, north and south poles. G_p and G_g: direction of the proper motion of Solar System and of the motion of the System relative to the neutral gas [23].

TABLE XII. – *Sidereal harmonic vectors at conjugate station* ($\delta = -36.1°$) *for Mt. Norikura* ($\delta = 36.1°$), *inferred from three types of anisotropy.*

		a^1		a^2		a^3	
		amplitude (%)	phase (h)	amplitude (%)	phase (h)	amplitude (%)	phase (h)
Norikura ($\delta = 36.1°$)		0.0548	0	0.0341	6	0.0092	0
Conjugate station ($\delta = -36.1°$)	I [a]	0.1250	0	0.0557	6	0.0092	0
	II [a]	0.0136	0	0.0047	6	0.0092	0
	γ-ray source [b]	0.0548	12	0.0341	6		

(a) From the anisotropy given in table XI.
(b) Inferred from the γ-ray source hypothesis (Alexeenko and Navara [19]).

considerably different sidereal variation at the conjugate station ($\delta = -36.1°$) for Mt. Norikura. Table XII shows two sets of harmonic vectors expected from the anisotropies in table XI. Except for a^3, the vectors at the conjugate station are greater or less than the corresponding vectors at Mt. Norikura, depending on the plus or minus sign of δ_R. In the table, there is one more set of harmonic vectors at $\delta = -36.1°$ inferred from the γ-ray origin hypothesis suggested by Alexeenko and Navara [19]. They assume that the sidereal variation in the energy region of $\sim 10^{13}$ eV is caused by γ-rays which are concentrated in the galactic equatorial plane. Based on this assumption, they explained the sidereal daily variation at Baxan shown in fig. 18. Such a space distribution of the γ-ray source can be approximately expressed by the second ($n = 2$) order term in eq. (22) with negative η_2-value and with its reference axis perpendicular to the galactic equatorial plane and therefore it produces a_2^1 and a_2^2 only. As $a_2^1(\eta_2, \theta_R, \theta)$ is North-South asymmetric ($a_2^1(\eta_2, \theta_R, \theta) = -a_2^1(\eta_2, \theta_R, \pi - \theta)$) with respect to θ, the amplitude of the expected vector (a^1) at the conjugate station ($\delta = -36.1°$) is the same as that at Mt. Norikura, but its phase must be different from the latter's by 12 hours. This distribution also is clearly different from the other two in the table. For the determination of a reliable structure and its origin, it is necessary to use those data at conjugate station in the southern hemisphere. In this respect, it is very important to promote observation at a conjugate station in the southern hemisphere.

The energy spectrum of the anisotropy responsible for the sidereal first and second harmonic vectors has been studied by the aid of the 36-fold air showers (^{36}F). Figure 27 shows the comparison of the vectors of ^3F and ^{36}F on the harmonic dial, and fig. 28 shows the amplitude of the first harmonic vector as a
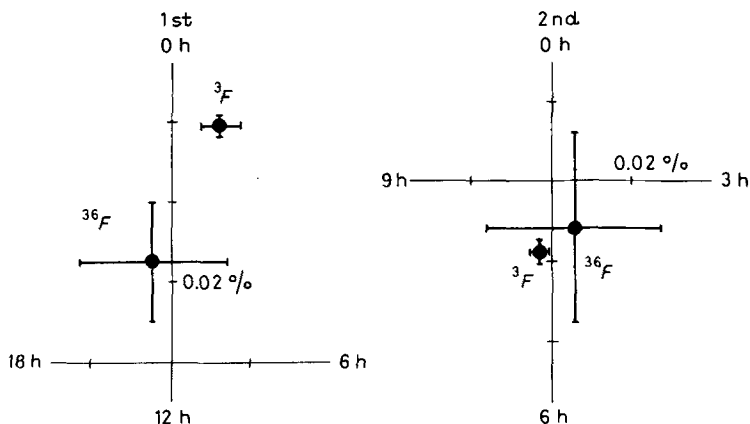
Fig. 27. – Comparison of sidereal first and second harmonic vectors of ^3F and ^{36}F.
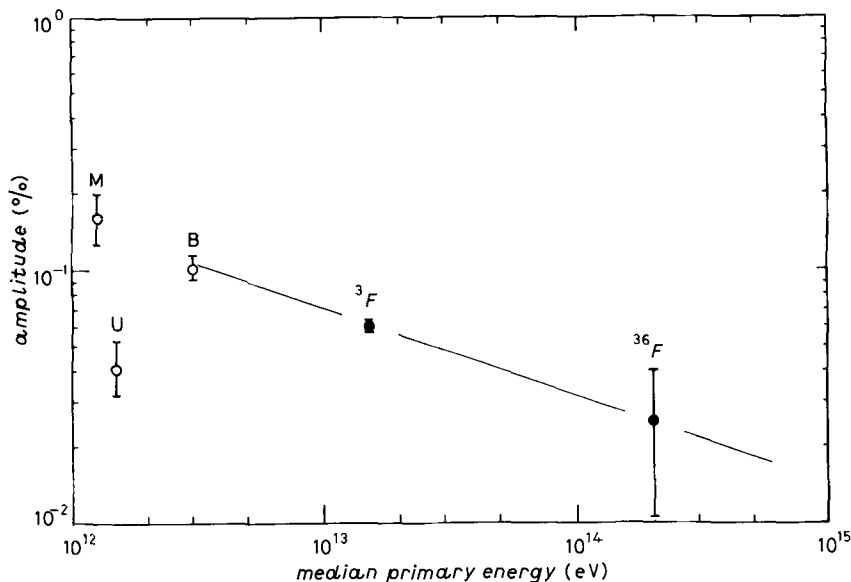
Fig. 28. – Energy dependence of sidereal first harmonic vector. B, M and U: underground muon observations. B: Baxan [43.4° N, 42.7° E; $E \geqslant 2000$ GeV; Andreyev et al. [28]]. M: Matsushiro [36.9° N, 138.1° E; $E_m \sim 1250$ GeV; Mori et al. [29]]. U: Utah [40.6° N, 111.5° W; $E_m \sim 1500$ GeV; Cutler et al. [30]].

[28] Yu. M. ADREYEV, A. E. CHUDAKOV, V. A. KOZYARIVSKY, A. M. SIDORENKO, T. I. TULUPOVA and A. V. VOEVODSKY: Proceedings of the XX International Cosmic Ray Conference, Moscow, 1987, 2, 22.

[29] S. MORI, S. SAGISAKA, S. YASUE and M. ICHINOSE: Proceedings of the XX International Cosmic Ray Conference, Moscow, 1987, 4, 160.

[30] D. J. CUTLER, H. E. BERGESON, J. F. DAVIS and D. E. GROOM: Astrophys. J., 248, 1166 (1981).

function of the median energy of air showers. If we simply assume the power-law spectrum of the amplitude, we get the power exponent of $\gamma \sim -0.3$ as shown in fig. 28. It is emphasized however that the logarithmic representation of the amplitude is a kind of trick to show the statistically insignificant amplitude like a significant one. This applies also to the present case of the amplitude of ^{36}F. As can be seen in fig. 27, the error for ^{36}F is so large that it almost covers the origin of the harmonic dial. Therefore, the existence of the first-order anisotropy itself is doubtful in this case and cannot discuss the spectral exponent. But, it is possible to estimate at least the probability that $^{36}F^1$(SI) would be comparable with $^3F^1$(SI). As their difference is 2.4 times as large as the error, the probability is only 1.6%. On the basis of the above consideration, it is concluded that although the spectral exponent cannot be determined, the galactic anisotropy responsible for the first harmonic vector in the energy region of $(10^{13} \div 10^{15})\,\mathrm{eV}$ seems to decrease its magnitude with the increase of energy. This conclusion is contradictory to the conventional one that the energy spectrum is flat or slightly increases with the increase of energy [3,4,31]. According to the present version, the anisotropy in the energy region $< 10^{15}\,\mathrm{eV}$ is supposed to belong to a category quite different from that in higher-energy region where the anisotropy seems to increase rapidly with the increase of energy. The present version as to the spectral exponent seems to be supported by the underground muon observations in comparatively high-energy region $(E_m \geqslant 10^{12}\,\mathrm{eV})$. As can be seen in fig. 28, the amplitudes of the sidereal first harmonic vector in this energy region are almost equal to or rather greater than the amplitude of ^3F.

Now, we discuss the polarity dependence of the harmonic vectors. As mentioned previously, if the galactic anisotropy is produced by the charged cosmic rays, the anisotropy in the rigidity region less than $10^{13}\,\mathrm{V}$ is subject to the heliomegnetic modulation and as a result, the observed sidereal variation arising from the anisotropy is subject to various kinds of the annual and semi-annual variation [20,21]. The modulation is predominant in the rigidity region $\sim 10^{12}\,\mathrm{V}$. As cosmic rays in this rigidity region can produce air showers (extensive air showers and local air showers) detectable with the present shower array, the observed sidereal variation might be subject to the modulation and show the polarity dependence in question. In the previous section, we have found some harmonic vectors showing such a polarity dependence. Among them, the most statistically significant polarity-dependent vector is $^3F^2$(SO) (cf. fig. 21 and 22). The vector reverses its phase from 6 hour to 0 hour at the transition period (1979-1980) of the polarity state. In association with this phase reversal, $^3D^2$(SO) also reverses its phase and furthermore, it always keeps its phase three hours earlier than that of $^3F^2$(SO) (cf. fig. 22). The phase relation between the two vectors certifies that $^3F^2$ is not of atmospheric origin but of solar or galactic

[31] L. C. TAN: *Proceedings of the XIX International Cosmic Ray Conference, La Jolla, 1985*, **2**, 318.

origin (cf. fig. 7). As for the solar origin hypothesis, there are two kinds of theory, one is the conventional one which explains the semidiurnal variation by the diffusion-convection of cosmic rays in interplanetary space [32], and the other explains it by the acceleration of cosmic rays in the neutral sheets of interplanetary magnetic field [33]. The solar semidiurnal variations produced by these mechanisms show some kinds of polarity dependence, but their phases are basically 3 hours on the average and are quite different from the observed phase of 0 hour or 6 hour.

Next, we discuss the galactic origin hypothesis. First of all, we have to disregard the γ-ray origin hypothesis as γ-rays are not subject to any heliomagnetic modulation. We assume that the anisotropy is produced by charged particles. If cosmic rays have very high energy, the heliomagnetic modulation is negligibly small and the sidereal variations can be expressed by eqs. (23) and (25). In this case, any anisotropy with order n cannot produce the harmonic variations with sideband frequencies ($f = 366m \pm k$ cycle/year; $m = 1, 2$; $k = 1, 2, \ldots$), such as solar diurnal variation (365 cycle/year). On the contrary, in case of low-energy cosmic rays, the anisotropy produces the variations of sideband frequencies owing to its heliomagnetic modulation. That is, the second ($n = 2$) order anisotropy $\eta_2 P_2^0(\cos\chi)$ can produce not only $\boldsymbol{a}_2^2(\mathrm{SI})$ but also the semidiurnal variations $\boldsymbol{a}_{n=2}^2(\mathrm{SI}_{1/2}, \mathrm{SO}, \text{etc.})$ and furthermore the first ($n = 1$) order anisotropy $\eta_1 P_1^0(\cos\chi)$ also can produce the semidiurnal variations $\boldsymbol{a}_{n=1}^2(\mathrm{SI}, \mathrm{SI}_{1/2}, \mathrm{SO}, \text{etc.})$ together with the diurnal variations $\boldsymbol{a}_{n=1}^1(\mathrm{SI}, \mathrm{SO}, \text{etc.})$ [20]. These modulation-produced variations are at the most several tenth of the corresponding mother variations $\boldsymbol{a}_1^1(\mathrm{SI})$ and $\boldsymbol{a}_2^2(\mathrm{SI})$, as

$$
(33) \quad \left\{
\begin{array}{l}
\left.\begin{array}{l}
|\boldsymbol{a}_1^2(\mathrm{SI}, \mathrm{SI}_{1/2}, \mathrm{SO}, \text{etc.})| \,/\, |\boldsymbol{a}_1^1(\mathrm{SI})| \\[4pt]
|\boldsymbol{a}_1^1(\mathrm{SO}, \text{etc.})| \,/\, |\boldsymbol{a}_1^1(\mathrm{SI})|
\end{array}\right\} \approx r_{\mathrm{M}}(\equiv \text{several} \cdot 10^{-1}), \\[20pt]
\left.\begin{array}{l}
|\boldsymbol{a}_2^1(\mathrm{SO}, \text{etc.})| \,/\, |\boldsymbol{a}_2^2(\mathrm{SI})| \\[4pt]
|\boldsymbol{a}_2^2(\mathrm{SI}_{1/2}, \mathrm{SO}, \text{etc.})| \,/\, |\boldsymbol{a}_2^2(\mathrm{SI})|
\end{array}\right\} \approx r_{\mathrm{M}}(\equiv \text{several} \cdot 10^{-1}),
\end{array}
\right.
$$

in which r_{M} is called the modulation rate. As the observed sidereal diurnal variation is greater than the corresponding semidiurnal variation, those variations for $n = 1$ would be greater than those for $n = 2$. In the following discussion, we neglect the effect of the second-order ($n = 2$) anisotropy. The first-order ($n = 1$) anisotropy with reference axis of α_{R} and δ_{R} can be decomposed into three components in the equatorial coordinates (X, Y, Z); X-and Y-com-

[32] K. MUNAKATA and K. NAGASHIMA: *Proceedings of the XIX International Cosmic Ray Conference, La Jolla, 1985*, **5**, 98.
[33] J. KOTA: *J. Phys. A*, **8**, 1349 (1975); G. ERDÖS and J. KOTA: *Astrophys. and Space Sci.*, **67**, 45 (1980).

ponents are, respectively, in the directions of $\alpha = 0$ hour and 6 hour in the equatorial plane and expressed by $\eta_1 P_1^1(\cos \delta_R) P_1^1(\cos \delta) \cos(2\pi/24)\alpha$ and $\eta_1 P_1^1(\cos \delta_R) P_1^1(\cos \delta) \sin(2\pi/24)\alpha$, while Z-component is parallel to the North Pole $(\delta = 90°)$ and expressed by $\eta_1 P_1^0(\cos \delta_R) P_1^0(\cos \delta)$ (cf. eqs. (23) and (25)). We express those vectors produced, respectively, by X, Y or Z component of the anisotropy as $a_{n=1}^m(\text{SI}, \ldots | X, Y \text{ or } Z)$. As the observed sidereal first harmonic vector $^3F^1(\text{SI})$ has the phase of $0 \div 1$ hour, we neglect in the following discussion the contribution of Y-component and consider only that of X-and Z-components. We first discuss the contribution of X-component to the observed $^3F^2(\text{SO})$. According to Nagashima et al.[20] and Nagashima and Morishita[21], the component could produce $^3F^2(\text{SO})$ in the low-energy region $(< 10^{13}\,\text{eV})$ with its phase of ~ 6 hour in the positive polarity state and of ~ 0 hour in the negative state in the northern hemisphere $(\delta > 0)$ (cf. eq. (25)). The phase exactly coincides with the observed phase shown in fig. 20. The characteristics of the expected $^3F^2(\text{SO})$ are as follows: 1) its phase is very stable against the change of the heliomagnetospheric circumstance, such as of the boundary radius of the magnetosphere, of the heliographic latitudinal extent (Λ_0) of the wavy neutral sheet and of the magnitude of IMF. Owing to the phase stability, we could observe very clear polarity dependence as shown in figs. 21 and 22. 2) The vector reverses its phase on the harmonic dial for the sign change of δ, in other words, the vector is North-South asymmetric and becomes zero for $\delta = 0$. On the contrary, the vector of solar origin hypotheses mentioned previously is even function of δ. Therefore, one could use the difference of character for the determination of the origin of the observed solar semidiurnal variation. In this respect, the observation in the southern hemisphere is most desirable.

The X-component could also explain the observed polarity dependence of $^3F^2(\text{SI})$ shown in fig. 23. Generally, the main part of $^3F^2(\text{SI})$ is the mother vector $a_2^2(\text{SI})$ produced mainly by the second $(n = 2)$ order anisotropy. Superposed on it, we could observe an additional vector $a_1^2(\text{SI}|X)$ produced by the X-component of the first-order $(n = 1)$ anisotropy. The additional vector has a phase of ~ 3 hour in P-state and of ~ 9 hour in N-state in the northern hemisphere $(\delta > 0)$. Therefore, the resultant vector at $\delta > 0$ could rotate its phase clockwise from P-state to N-state as observed (cf. fig. 23) and the difference vector $^3F^2(\text{SI}|P - N)$ could have almost the same phase (~ 3 hour) as observed (cf. fig. 21). The characteristics of the additional vector $a_1^2(\text{SI}|X)$ produced by the X-component are the same as those of $a_1^2(\text{SO}|X)$ mentioned previously. Owing to the North-South asymmetric character with respect to δ, the resultant vector in the southern hemisphere $(\delta < 0)$ would rotate its phase counterclockwise from P-state to N-state and the difference vector $^3F^2(\text{SI}|P - N)$ would have a phase of ~ 9 hour. Therefore, in this case also, the observation in the southern hemisphere is effective for the determination of the origin of the polarity dependence. The mother vector for those vectors discussed in the above is $a_1^1(\text{SI}|X)$ which is observed as $^3F^1(\text{SI})$. As can be seen in fig. 23, this vector shows some slight phase change for the polarity

reversal, although it is not statistically well significant. It is noted that this phase change also could be explained by the polarity dependence of $a_1^1(\mathrm{SI}|X)$ derived from the X-component [20,21].

In the above discussion, we did not mention the effect of the Z-component. This component also produces the polarity-dependent harmonic vectors $a_1^1(\mathrm{SI}, \mathrm{SO}, \mathrm{AS}, \text{ etc. }|Z)$ and $a_1^2(\mathrm{SI}, \mathrm{SI}_{1/2}, \mathrm{SO}, \text{ etc. }|Z)$. These vectors have almost the same character as that of the corresponding vectors $a_1^1(\mathrm{SI}, \mathrm{SO}, \mathrm{AS}, \text{ etc. }|X)$ and $a_1^2(\mathrm{SI}, \mathrm{SI}_{1/2}, \mathrm{SO}, \text{ etc. }|X)$. For example, the phases of the corresponding vectors from X-and Z-components are both stable or both unstable depending on the kind of harmonics (SI, ...). The different points to be noted are that 1) the vectors from Z-component are odd function of δ_{R} while those from X-component are even function and 2) the corresponding stable vectors from X-and Z-components are nearly perpendicular to each other on the harmonic dial. Owing to this phase difference, the vectors from Z-component are quite different from the corresponding observed vectors. This fact indicates that the contribution of Z-component of the anisotropy is very small and the anisotropy is in the direction near the equatorial region ($|\delta_{\mathrm{R}}| \ll 90°$), as expected from the determination of the space distribution.

As above, we have demonstrated that some of the polarity-dependent vectors could be explained by the heliomagnetic modulation of the first-order anisotropy. But the explanation so far presented is only qualitative, and the quantitative explanation of their amplitude of the order of 0.01% is next required. As the contribution of cosmic rays in the energy region of $\simeq 10^{12}\,\mathrm{eV}$ to the air shower flux is about ten percent and also as the modulation rate r_{M} in eq. (33) is no more than several tens percent, their mother vector $a_{n=1}^1(\mathrm{SI})$ in the energy region of $\sim 10^{12}\,\mathrm{eV}$ must be about $(0.5 \div 1.0)\%$ for the explanation of the observation ($\sim 0.01\%$). This estimated magnitude of $a_1^1(\mathrm{SI})$ could be reduced if the heliomagnetic modulation is strengthened by the increase of IMF [21]. But, at any rate, the galactic anisotropy in the region of $(10^{12} \div 10^{13})\,\mathrm{eV}$ must have a power-law spectrum with negative exponent. This seems consistent with the previous estimate of the spectrum in the high-energy region of $(10^{13} \div 10^{15})\,\mathrm{eV}$ and it seems also not contradictory to the amplitudes of the sidereal time variations in low-energy region $\sim 10^{12}\,\mathrm{eV}$ obtained by muon observations at deep underground stations, shown in fig. 28. Although these amplitudes in the low-energy region are a little smaller than the required amplitude of $a_1^1(\mathrm{SI}|X)$ estimated in the above, the difference of this much might be permissible by the following reasons: 1) the present estimate of the required amplitude is only approximate and 2) the signal from the anisotropy will be attenuated at these stations as the anisotropy sharply decreases in the energy region $< 10^{12}\,\mathrm{eV}$ with the decrease of energy owing to the heliomagnetic modulation [20,21,34]. According to the present

---

[34] S. YASUE, I. MORISHITA and K. NAGASHIMA: *Planet. Space Sci.*, **33**, 1057 (1985).

assumption, the sidereal daily variation in this energy region ($\geqslant 10^{12}$ eV) must show dominant polarity dependence as discussed in the above. Unfortunately, however, owing to the recent start of the observations, the polarity reversal has not been experienced by the observations at these stations ($\geqslant 10^{12}$ eV). We have to wait the result of the polarity dependence of the vector until the next reversal time. In much lower-energy region < 700 GeV, there have been many observations on the sidereal time variation for many years [1,29]. But, except for an extremely low-energy region [35], one cannot find any signals of the expected change of the variation due to the polarity reversal. Especially, Bercovitch [36] tried to test the effect of the polarity reversal using his data of the Ottawa horizontal muon array, its median energy being as high as 660 GeV. But, he could not find any indication of it and suggested that some modification is necessary of the structure of the heliomagnetosphere adopted by Nagashima *et al.* [20]. These results in lower-energy region seem to be contradictory to the present result. There is no reasonable explanation for it, except that the observed sidereal variations in two energy regions divided at $\sim 10^{12}$ eV have different origins from each other or the observed results are not yet statistically significant enough to test their origin.

As above, we have pointed out the existence of the galactic anisotropy in the energy region of $\sim 10^{13}$ eV and also the existence of the heliomagnetic modulation of the galactic anisotropy in the energy region of $\sim 10^{12}$ eV. The finding of the polarity dependence of the sidereal variation of galactic origin has given rise to some troublesome question on the origin of the galactic anisotropy in both low- and high-energy regions. It is emphasized however that without the confirmation of the dependence, one cannot definitely determine the origin of the anisotropy and also the overall structure of the heliomagnetosphere. In this respect, other independent observations are important to be performed, especially in the southern hemisphere.

* * *

[35] G. CINI-CASTAGNOLI, D. MAROCCHI, H. ELLIOT, R. G. MARSDEN and T. THAMBYAHPILLAI: *Proceedings of the XIV International Cosmic Ray Conference, München, 1975*, 4, 1453; R. G. MARSDEN, H. ELLIOT, R. J. HYNDS and T. THAMBYAHPILLAI: *Nature*, **260**, 491 (1976); M. ICHINOSE and K. MURAKAMI: *Proceedings of the International Symposium on High Energy Cosmic Ray Modulation, Tokyo, Japan, 1976*, 291; T. THAMBYAHPILLAI: *Proceedings of the XVIII International Cosmic Ray Conference, Bangalore, 1983*, 3, 383.
[36] M. BERCOVITCH: *Proceedings of the International Symposium on Cosmic Ray Modulation in the Heliosphere, Morika, Japan, 1984*, 329.

Observatory and also to the staff of Cosmic-Ray Research Laboratory, Nagoya University; Messrs. M. Orito and T. Yamada and Mrs. M. Hayase for the maintenance of the air shower observation and Mrs. H. Satake and Miss S. Demura for preparing the manuscript. All the computations in this work were made at the Computer Center, Nagoya University and the Computer Centre, Institute of Plasma Physics, Nagoya University.

● RIASSUNTO (*)

Sono stati osservati sciami cosmici estensivi (EAS) con energia primaria mediana (E_m) di ($10^{13} \div 10^{15}$) eV dal 1970 a Mt. Norikura (2770 m, latitudine geografica 36.1° N, longitudine 137.6° E) per studiare una variazione giornaliera siderale dei raggi cosmici di origine galattica. Si riporta una sintesi dei risultati osservati. EAS mostra una significativa variazione siderale diurna con ampiezza (0.060 ± 0.03)% e fase (0.8 ± 0.3) h in tempo locale siderale per $E_m \sim 1.5 \cdot 10^{13}$ eV. Le variazioni siderali semi e tri-diurne sono risultate anch'esse statisticamente significative. Si prova che queste variazioni sono d'origine galattica con un metodo che utilizza la differenza tra due osservazioni di sciami cosmici direzionali (est e ovest). Si trova che queste variazioni sono soggette, come previsto da Nagashima *et al.*, alla variazione annuale dovuta alla modulazione eliomagnetica dell'anisotropia galattica, che domina nella regione di rigidità $\sim 10^{12}$ V e inoltre che la variazione annuale cambia fase a causa dell'inversione di polarità del campo magnetico polare del Sole, che si verifica nel periodo di massima attività solare. Ciò indica che l'anisotropia è prodotta da raggi cosmici carichi, contrariamente a quanto previsto dall'ipotesi sull'origine da raggi gamma, suggerita da Alexeenko e Navara. Con l'aumento di E_m, l'anisotropia sembra ridursi in quanto non siamo riusciti a rilevare una variazione siderale significativa in EAS con $E_m \sim 2 \cdot 10^{14}$ eV. Questo risultato sembra in contraddizione con la conclusione convenzionale che lo spettro di energia dell'anisotropia è piatto o cresce appena con l'energia.

(*) *Traduzione a cura della Redazione.*

Анизотропия галактических космических лучей и ее модуляция в гелиомагнитосфере, полученные из результатов наблюдений атмосферных ливней на г. Норикура.

Резюме (*). — Широкие атмосферные ливни со средней первичной энергией (E_m), равной ($10^{13} \div 10^{15}$) эВ, наблюдались с 1970 года на г. Нарикура (2770 м над уровнем моря; географическая широта 36.1° N, долгота 137.6° E), с целью исследовать суточное изменение сидерических космических лучей галактической природы. Предлагается обзор полученных результатов. Широкие атмосферные ливни обнаруживают значительное сидерическое суточное изменение с амплитудой (0.060 ± 0.003)% и фазой 0.8 ± 0.3 часа сидерического локального времени для $E_m \sim 1.5 \cdot 10^{13}$ эВ. Сидерические полу- и трех-суточные изменения являются также статистически заметными. Доказывается, что эти изменения имеют галактическое происхождение. Этот результат получен с помощью метода, который использует

разности при наблюдениях атмосферных ливней в двух направлениях (в восточном и западном направлениях). Получено, что эти вариации подчиняются, как было предсказано Нагашима и др., годовому изменению, обусловленному гели-омагнитосферной модуляцией галактической анизотропии, которая доминирует в области жесткости $\sim 10^{12}$ D, и кроме того, годовая вариация изменяет фазу, в связи с реверсированием полярности магнитного поля Солнца, котороепроисходит в период максимума солнечной активности. Этот результат показывает, что возникает анизотропия, вызванная заряженными космическими лучами, в противоположность предсказанию Алексеенко и Навара, связанному с гипотезой происхождения γ-лучей. При увеличении E_m анизотропия, повидимому, уменьшается, так как мы не смогли зарегистрировать какого-либо существенного сидерического изменения в широких атмосферных ливнях в случае $E_m \sim 2 \cdot 10^{14}$ эВ. Это противоречит общепринятому заключению, что энергетический спектр анизотропии является пологим или слегка увеличивается с энергией.

(*) *Переведено редакцией.*